Differential cross-section measurements for the $^{9}Be(^{3}He,^{3}He_{0})^{9}Be$ elastic scattering and the $^{9}Be(^{3}He,p_{x})^{11}B$ reactions

V. Foteinou[1,*], F. Maragkos[1,2], H.-W. Becker[1], L. Hess[3], K. Ivanković[4], M. Kokkoris[2], M. Mayer[3], G. Provatas[4], D. Rogalla[1]

[1]*Central Unit for Ion Beams and Radionuclides, Ruhr University Bochum, 44801 Bochum, Germany*

[2]*Department of Physics, National Technical University of Athens, 15780 Athens, Greece*

[3]*Max-Planck-Institut for Plasma Physics, 85748 Garching, Germany*

[4] *Division of Experimental Physics, Ruđer Bošković Institute, 10000 Zagreb, Croatia*

Abstract

The differential cross sections of $^{9}Be(^{3}He,^{3}He_{0})^{9}Be$ elastic scattering and of the $^{9}Be(^{3}He,p_{0,1,2,3,4+5,6,7})^{11}B$ reactions have been determined in the energy range from 1.6 to 6 MeV at six backward angles from 120° to 170°, with a step of 10°. The experiments were performed at the 4 MV Dynamitron Tandem Laboratory of the Central Unit for Ion Beams and Radionuclides of the Ruhr University Bochum in Germany. The obtained datasets have been validated through benchmarking experiments, at 8 beam energies, using a thick, high-purity, beryllium foil. The results of the present work are compared with existing ones from literature and any discrepancies observed are discussed.

Keywords: ^{3}He-NRA; ^{3}He-EBS; ^{9}Be; Differential cross sections

PACS: 82.80.Yc, 25.55.-e, 25.55.Ci

* Corresponding author: Varvara.Foteinou@rub.de

1. Introduction

Beryllium is a very light and relatively rare metal that occurs in nature only as a mineral component. It consists of a single stable isotope, ^{9}Be, and small traces of ^{7}Be and ^{10}Be. Despite its low atomic number and density, beryllium is characterized by exceptional physical properties, such as superior thermal stability and conductivity, high flexural rigidity and high melting point. Due to these properties, beryllium finds numerous applications, particularly in telecommunications, aerospace and defense industries. In addition, beryllium has a relatively high neutron scattering cross section and acts as an oxygen getter, properties that, combined with its high melting point and low atomic number, render beryllium one of the most important materials for plasma-facing components in controlled fusion devices [1,2]. It has been used extensively in JET [3], and is currently being foreseen as wall material for ITER. Hence, the accurate quantitative determination and depth profiling of beryllium is of crucial importance.

Ion beam analysis (IBA) techniques, particularly nuclear reaction analysis (NRA) and elastic backscattering spectroscopy (EBS), have been proven to be ideal for the quantitative analysis of almost all light elements. NRA is additionally characterized by high isotopic selectivity, enhanced sensitivity for many elements and the possibility of simultaneous analysis of several light elements in near–surface layers of materials with the proper choice of probing beam, such as deuterons or ^{3}He ions. Several studies to date have focused on the study of deuteron-induced reactions and elastic scattering, establishing a rather rich literature of differential cross-section data suitable for d-EBS and d-NRA applications. Nevertheless, there are applications in which the use of deuterons as probing beam should be avoided. In fusion energy research, for example, deuterium is one of the key elements that must be quantified in the components facing the plasma. Consequently, the use of a deuteron beam should be prevented, rendering ^{3}He beams the best candidate for these studies [4]. Moreover, although the probing depth of deuteron beams is significantly higher when compared to ^{3}He beams, the depth resolution using (d,p) reactions is usually limited due to the low stopping powers for deuterons and protons, while (^{3}He,p) reactions can provide good depth resolution due to the higher stopping power of He ions.

The implementation of ^{3}He-NRA and ^{3}He-EBS is, however, severely impeded by the lack of reliable cross-section data in literature, over a wide range of energies and detection angles suitable for IBA applications (θ≥120). Specifically, for the ^{3}He elastic scattering on ^{9}Be, the only datasets available in literature are those by Bondouk et al [5], covering a restricted energy range and only three detection angles. For the $^{9}Be(^{3}He,p_0)^{11}B$ and $^{9}Be(^{3}He,p_1)^{11}B$ reaction channels, there are three differential cross-section datasets available, the data by Wolicki et al. [6], Barradas et al. [7] and Provatas et al. [8]. However, these datasets exhibit significant discrepancies, which will be discussed in more detail in the following sections. For the $^{9}Be(^{3}He,p_2)^{11}B$ and $^{9}Be(^{3}He,p_3)^{11}B$ reactions, there exist the datasets by Barradas et al. [7] and Provatas et al. [8], which also present significant discrepancies. Concerning the reactions $^{9}Be(^{3}He,p_{4+5})^{11}B$ and $^{9}Be(^{3}He,p_6)^{11}B$, the only available datasets in literature are those by Provatas et al. [8], while no data have been reported to date for the $^{9}Be(^{3}He,p_7)^{11}B$ reaction.

2. Experimental setup

The cross-section and benchmarking measurements, as well as the target analysis, were carried out at the 4 MV Dynamitron Tandem Laboratory of the Central Unit for Ion Beams and Radionuclides (RUBION) of the Ruhr University Bochum in Germany. In order to minimize systematic errors, additional benchmarking experiments were carried out at the Tandem Accelerator Facility of the Ruđer Bošković Institute (RBI) in Zagreb, Croatia.

For the cross-section measurements, the ^{3}He beams were accelerated in the energy range from 1600 to 6000 keV, in steps of 50 or 100 keV. The benchmarking experiments at RUBION were performed at 1.9, 2.5, 3.0, 3.7, 4.4, 5.2 and 6.0 MeV, and at RBI at 2.3 and 3 MeV. For the calculation of the final beam energy at RUBION, the magnetic constant of the analyzer magnet was determined by nuclear magnetic resonance measurements (NMR), in particular by the measurement of the 992-keV resonance of the $^{27}Al(p,\gamma)^{28}Si$ reaction. The determined magnetic constant is consistent with a previous study performed in 2021 at the RUBION laboratory, which comprised 42 measurements of 7 different resonances [9]. The effective energy of the beam was calculated considering the energy loss within the target by means of the SIMNRA v. 7.03 code [10] employing the SRIM2013 [11] stopping power data.

The experimental setup used in the cross-section and benchmarking measurements at RUBION is presented in Fig. 1. The ^{3}He beam was directed into a cylindrical scattering chamber (diameter ~ 50 cm) through a 3-mm and a 1-mm tantalum collimator respectively located at a distance of 73 and 30 cm from the target. The beam-spot diameter was ~2 mm, while the current did not exceed 20 nA in order to prevent the loss of target material due to heating and to minimize the dead time (< 0.5 %). The detection setup consisted of six silicon surface barrier (SSB) detectors of 1500 μm in thickness, placed on a high-precision goniometer (0.1°) at 120°, 130°, 140°, 150°, 160° and 170°, with respect to the beam direction and at a distance of ~7.5 cm from the target. Orthogonal tantalum slits (~4×8 mm^2) were placed in front of the detectors in order to reduce the azimuthal angular uncertainty (< ±1.5°) while allowing an acceptable effective solid angle to be subtended by the detectors (~5 msr). Cylindrical aluminum tubes with length of 3.4 cm and an inside diameter of 1.1 cm were additionally placed in front of the detectors to reduce the background due to scattering on the chamber walls and/or the Faraday cup. The vacuum was maintained throughout all measurements at ~$5x10^{-7}$ Torr. A typical spectrum collected at E_{lab}=2518 keV and θ=160° is presented in Fig. 2a and Fig. 2b. The former corresponds to the high-energy part of this spectrum, while the latter to the low-energy part.

The target used for the differential cross-section measurements was commercially manufactured (Lebow Company) and consisted of two thin layers, the Be layer (~200 nm) and a ~100-nm Cu substrate. An ultra-thin Au film (~3 nm) was evaporated in RUBION onto its surface for normalization purposes and to ensure thermal stability. A thick, high-purity (>99,8 %) Be film was used for the benchmarking experiments. For normalization purposes, a thin Au film (~10 nm) was evaporated on its surface as well.

3. Data Analysis

In order to avoid errors in the measurement of the beam current and the solid angle covered by each detector, the differential cross sections presented in this work were determined with respect to the Rutherford ones for the elastic scattering on Au. It is worth mentioning here that the use of the Au scattering peak was adopted because the background underneath the Cu peak was more complicated. In a few cases, however, the Au scattering peak overlapped with one or more lower-energy peaks of the $^{9}Be(^{3}He,p_{x})^{11}B$ reaction. In these cases, the reported differential cross sections were determined relatively to the cross sections of the elastic scattering on Cu, which also follows the Rutherford formula at the beam energies employed. More specifically, the following expression was used:

$$\left(\frac{d\sigma}{d\Omega}\right)_{E,\theta}^{Be} = \left(\frac{d\sigma}{d\Omega}\right)_{E',\theta}^{x,Ruth} \times \frac{Y_{Be}}{Y_x} \times \frac{N_x}{N_{Be}}$$

where E and E′ correspond to the beam energies at half of Be layer and half of Au (or Cu) layer, respectively, θ is the detection angle, Y_{Be} is the integrated area of the respective Be peak, Y_x the integrated area of the Au (or Cu) scattering peak, N_x/N_{Be} is the ratio of the total number of Au (or Cu) versus Be nuclei in the target and $\left(\frac{d\sigma}{d\Omega}\right)_{E',\theta}^{x,Ruth}$ is the screening-corrected differential cross section for the elastic scattering of ^{3}He from Au (or Cu) at beam energy E′ and detection angle θ.

The total thicknesses of Be, Cu, and Au were determined by d-EBS and α-EBS measurements at 1785 and 3780 keV, respectively, and for the scattering angle of 160°. These energies were chosen because in each case there are three differential cross-section datasets available in the literature that, despite the small differences in the detection angle, are in almost absolute agreement. In particular, for the $^{9}Be(d,d_0)^{9}Be$ elastic scattering there are the datasets by Ntemou et al. [12] at θ=160°, Machali et al. [13] at θ=156° and Renken et al. [14] at θ=158.9°, while for $^{9}Be(\alpha,\alpha_0)^{9}Be$, the data by Lombardo et al. [15] at θ=160°, Liu et al. [16] at θ=165° and Leavitt et al. [17] at θ=170.5°. The spectra collected from these measurements are presented in Figs. 3a-b, along with the simulated ones. In both cases, the analysis was performed by means of the SIMNRA v. 7.03 code employing the SRIM2013 stopping power data, the straggling model of Chu and Yang and the differential cross-section data of Ntemou et al. [12] for $^{9}Be(d,d_0)^{9}Be$ and Lombardo et al. [15] for $^{9}Be(\alpha,\alpha_0)^{9}Be$, which, among the aforementioned, are the only ones at 160°. Based on the d-EBS measurement, the total absolute thicknesses of Be, Cu, and Au were determined respectively to $(2390\pm210)\cdot10^{15}$ at/cm^2, $(845\pm70)\cdot10^{15}$ at/cm^2 and $(21.0\pm1.7)\cdot10^{15}$ at/cm^2. The reported uncertainties include the errors in the measurement of the beam current and the solid angle, the uncertainty of the differential cross sections employed [12] and the statistical errors in the integration of the experimental peaks. These values coincide perfectly with the nominal ones specified by the manufacturers ($2450\cdot10^{15}$ at/cm^2 for Be and $845\cdot10^{15}$ at/cm^2 for Cu). The resulting ratios N_{Au}/N_{Be} and N_{Cu}/N_{Be} are consequently equal to 0.0088±0.0004 and 0.354±0.013, respectively. These ratios differ only slightly from those obtained by the α-EBS measurement, namely, 0.0089±0.0007 for N_{Au}/N_{Be} and 0.37±0.03 for N_{Cu}/N_{Be}. The weighted average values of the N_{Au}/N_{Be} and N_{Cu}/N_{Be} ratios were thus determined to 0.0088±0.0003 and 0.356±0.012. The errors reported above for the N_{Au}/N_{Be} and N_{Cu}/N_{Be} ratios include the quoted uncertainties of the experimental differential cross sections employed for the $^{9}Be(d,d_0)^{9}Be$ [12] and

$^{9}Be(\alpha,\alpha_0)^{9}Be$ [15] elastic scattering and the statistical errors from the integration of the corresponding peaks, however, they do not include the uncertainties in the implemented stopping power data, which, according to the SRIM website (http://www.srim.org/), have a minimum value of ~6% for beryllium. The high lateral homogeneity of the target was verified by α-EBS measurements at 3780 keV, by changing the position of the target. The differences in the yields of the Au, Cu and Be peaks did not exceed 3%. Finally, to ensure that no target deterioration occurred, the first measurement at Elab=1570 keV was repeated at the end of the experiment. The discrepancies between the initial and repeated measurement did not exceed the respective statistical uncertainties for the reactions under study in any case.

For the determination of the Y_{Be}, Y_{Au} and Y_{Cu} peak areas and the subtraction of the background, the TV code [18] was used. The statistical uncertainties in Y_{Au} and Y_{Cu} were below ~1%, while they varied between ~1.3% and ~11% for the peaks corresponding to the Be elastic scattering and the $^{9}Be(^{3}He,p_x)^{11}B$ reactions. It must be noted that, due to peak overlapping, the determination of Y_{Be} in specific cases was not possible. This issue was particularly evident in the $^{9}Be(^{3}He,^{3}He)$ ^{9}Be elastic scattering, with the corresponding peak overlapping over wide energy intervals with the peak of the $^{9}Be(^{3}He,d_2)^{10}B$ reaction and/or with lower-energy peaks of the $^{9}Be(^{3}He,p_x)^{11}B$ reaction channels. In addition, at certain beam energies, overlapping of the p_3, p_{4+5} and p_6 peaks with the $^{12}C(^{3}He,p_{0,1})^{14}N$ and $^{16}O(^{3}He,p_0)^{18}F$ reaction peaks was also observed. At higher beam energies, the p_6 and p_7 peaks overlapped completely with the Au elastic peak. Furthermore, the p_4 and p_5 peaks were not completely resolved in most of the collected spectra and were thus analyzed as one. The p_0, p_1, and p_2 peaks, by contrast, were completely isolated and nearly free of background over essentially the entire energy range studied.

4. Results and discussion

The differential cross-section values obtained in the present work varied between 0.13 and 1.74 mb/sr for the $^{9}Be(^{3}He,p_{0-7})^{11}B$ reactions, with an average total error of ~6%, and between 2.6 and 10.3 mb/sr for the $^{9}Be(^{3}He,^{3}He)$ elastic scattering, with a total estimated uncertainty that did not exceed 9%. A detailed description of all errors contributing to the total estimated uncertainty is given in Table 1. The error in the final beam energy was ~3 keV, including the accelerator energy ripple (0.4 keV), the uncertainty in the magnetic constant (0.07%) as determined in [9] and the beam straggling inside the target.

The results of the current work are given in Tables 1-8 in the Appendix and plotted in Figs. 4-11 (black dots), along with all data available in literature for detection angles close to those studied. In particular, for the ^{3}He elastic scattering on ^{9}Be (Figs. 4a-f), the only available datasets are those by Bondouk et al. [5] at 122°, 137° and 145° (red triangles). Wolicki et al. [6] report data for the $^{9}Be(^{3}He,p_0)^{11}B$ (Fig. 5) and $^{9}Be(^{3}He,p_1)^{11}B$ (Fig. 6) reactions at 120° and 150° (red open squares), while Barradas et al. [7] for the proton groups p_0-p_3 and for the scattering angle of 135° (blue open triangles in Figs. 5-8). The datasets by Provatas et al. [8] cover all proton groups up to p_6 and the detection angles from 107° to 164° with a step of 2° (green open dots). In the case of the $^{9}Be(^{3}He,^{3}He)$ elastic scattering, the overlap between the current datasets and those by Bondouk et al. is extremely limited, as can be observed in Fig. 4. In the restricted regions where these datasets do overlap, there is very good agreement, despite the small differences in the detection angle. Regarding the $^{9}Be(^{3}He,p_0)^{11}B$ and $^{9}Be(^{3}He,p_1)^{11}B$ reactions at 120° and 150°, the differential cross-section values obtained here agree well with those of Wolicki et al., at energies up to ~2 MeV for the $^{9}Be(^{3}He,p_0)^{11}B$ reaction and up to ~3 MeV for the $^{9}Be(^{3}He,p_1)^{11}B$ one, while discrepancies are observed at higher energies. These discrepancies could be attributed to the fact that the datasets of Wolicki et al. were determined by normalization to their own measurement at 2 MeV. In addition, Wolicki et al. provide no information about the thickness of the target used. An overall good agreement is also observed between the present data at 130° and 140° and those of Barradas et al. at 135° for all proton groups up to p_3. The datasets of Provatas et al., however, deviate from the present ones by a factor of ~0.7 for all proton groups and all scattering angles, for almost the entire energy range over which these datasets overlap. The one exception is essentially the $^{9}Be(^{3}He,p_2)^{11}B$ reaction at 170°, for which good agreement is observed at energies above ~2.1 MeV, but for lower energies there is still a difference of the order of ~30-40%. There is no obvious explanation for this deviation, aside from a possible systematic error in the current integration method or in the determination of the target thickness.

The differential cross-section values of each reaction studied in the present work are also plotted together in Figs. 12a-h to illustrate their angular variation, which, as can be observed, is quite strong in all cases and throughout nearly the entire energy range studied (factor of up to ~3). This strong angular distribution is related to the resonance structure of the reactions.

The cross-section errors presented in Figs. 4-12 include only the statistical errors resulting from the integration of the Be, Au, and Cu peak areas and the uncertainties from the determination of the Au/Be and Cu/Be thickness ratios. The errors reported in Tables 2-9 correspond to the total estimated uncertainties, including all statistical and systematic uncertainties stated in the previous section with the exception of the uncertainties in the implemented stopping power data. The authors decided to report also the total estimated uncertainties, thus following the procedure recommended in [19].

5. Benchmarking results

The differential cross sections obtained in this work were validated by measuring a target of infinite thickness at different energies and comparing the collected spectra with simulated ones calculated on the basis of the present results. These benchmarking experiments were carried out at

RUBION, Bochum and at RBI, Zagreb, using the same high-purity, thick Be foil, over which a thin Au film (~15 nm) was deposited. The exact thickness of the Au layer was determined at RUBION by RBS measurements using 1.0-MeV deuterons.

In the RUBION measurements the same detection setup as in the cross-section measurements was used, consisting of six 1500-μm thick SSB detectors, positioned at 10^o intervals between 120^o and 170^o, with respect to the beam direction. The measurements were performed at 7 beam energies, namely, 1.9, 2.5, 3.0, 3.7, 4.4, 5.2 and 6.0 MeV. In order to suppress the background arising from the $^{9}Be(^{3}He,\alpha_x)^{8}Be$ reactions, 125-μm Kapton foils were added in front of the detectors at θ=120°, 140°, 150°, 160° and 170° for all measurements except the one at 1.9 MeV. For the first measurement at 1.9 MeV, the products $Q\times\Omega_i$ (i=120°, 130°, 140°, 150°, 160°, and 170°) of the total beam charge Q and the solid angle subtended by each detector Ω_i were normalized to the elastic Au peak of the corresponding spectrum. For the remaining measurements, the charge was normalized to the Au peak at 130°, where no Kapton foil was added. The ratios Ω_i/Ω_{130} between the solid angles covered by the detectors at 120°, 140°, 150°, 160°, and 170° and the solid angle of the detector at 130° were determined with respect to the areas of the Au peaks in the spectra recorded at 1.9 MeV.

The measurements at RBI were performed at E=2.3 and 3.0 MeV using a 2000-μm SSB detector at θ=140°. A Mylar film with a thickness of 120 μm was placed for background suppression purposes to the front of the detector. For charge normalization, a second SSB detector of 300 μm in thickness was positioned at 135° to monitor the elastically backscattered beam particles from Au. To determine the ratio of the solid angles covered by the two detectors, a similar process as in the RUBION measurements was followed, by also collecting spectra without the Mylar foil covering the detector at 140°, in order to utilize the Au elastic peak.

The spectra collected in both measurements were analyzed using the SIMNRA v.7.03 code and employing the SRIM2013 stopping power data and the straggling model of Chu and Yang. Representative examples of the measurements at RUBION for a combination of various detection angles and beam energies are presented in Fig. 13, together with the two measurements performed at RBI. As can be observed, the agreement between the experimental and simulated spectra is very good, especially when considering that no background is subtracted from the experimental spectra. The discrepancies between the integrals of the simulated and the net experimental areas did not exceed 5%. In some cases, however, the signal-to-background ratio was extremely low, preventing the quantification of these discrepancies. These cases were hence disregarded. Characteristic examples are the p_7 peak in Fig. 13f and p_6 in Fig. 13g. In addition, the benchmarking for the differential cross sections of the ^{9}Be(^{3}He,^{3}He) elastic scattering was not possible as the corresponding continuum was suppressed by the Kapton foil in all spectra except in those collected at 1.9 MeV and those at 130° for the entire energy range. Even in these cases, however, the Be elastic continuum lies on a complicated background originating from various channels of the ^{9}Be(^{3}He,p_x)^{11}B, ^{9}Be(^{3}He,d_x)^{10}Be and ^{9}Be(^{3}He,α_x)^{8}Be reactions, the subtraction of which is not possible, since no evaluated differential cross-section datasets are available for these reactions.

6. Conclusions

In the present work the differential cross sections of the ^{9}Be(^{3}He,^{3}He$_0$)^{9}Be elastic scattering and the ^{9}Be(^{3}He,$p_{0,1,2,3,4+5,6,7}$)^{11}B reaction channels have been determined at six backward angles from 120° to 170°, with a step of 10°, and at energies from 1.6 to 6 MeV, in steps of 50 or 100 keV. The differential cross sections of all studied proton groups were below 1.8 mb/sr, but, nonetheless, the corresponding peaks and in particular the p_0, p_1, and p_2 ones arise in high-energy and nearly background-free regions and are therefore suitable for NRA applications. On the other hand, special attention is required when ^{3}He-EBS is employed for the analysis of beryllium, as the corresponding peak overlaps in extended energy regions with peaks from the ^{9}Be(^{3}He,d_x) and ^{9}Be(^{3}He,p_x) reactions. The obtained datasets were validated in two different laboratories through benchmarking experiments, revealing an agreement better than ~5% with the experimental spectra. The differential cross-section data obtained in this work will soon be available at the IBANDL website (https://www-nds.iaea.org/exfor/ibandl.htm).

Acknowledgements

This work was supported by the Deutsche Forschungsgemeinschaft DFG under the project FO 1383/2-1. We would like to thank the staff of the accelerator facilities of the Ruhr University Bochum and in particular Mr. Timo Wegener for his support during the measurements. One of the authors would also like to acknowledge the financial support from ELKE, NTUA. The co-author G.P. acknowledges the financial support from the European Regional Development Fund for the 'Center of Excellence for Advanced Materials and Sensing Devices' (Grant No. KK.01.1.1.01.0001).

Appendix

The differential cross-section values obtained in the present work for the ^{9}Be(^{3}He,^{3}He$_0$)^{9}Be elastic scattering and the ^{9}Be(^{3}He,$p_{0,1,2,3,4+5,6,7}$)^{11}B reactions are listed in the following tables.

References

[1] K. L. Wilson et al, J. Vac. Sc. Technol. 8 (1990) 1750

[2] V Philipps et al., Fusion Eng. Des. 85 (2010) 1581–1586

[3] S. Brezinsek, JET-EFDA contributors, J. Nucl. Mater. 463 (2015) 11

[4] M. Mayer et al., Nucl. Fusion 60 (2020) 025001

[5] I. Bondouk et al., Rev. Roum. Phys. 19 (1974) 653

[6] E. A. Wolicki et al., Phys. Rev. 116 (1959) 1585

[7] N. P. Barradas et al., Nucl. Instr. and Meth. in Phys. Res. B346 (2015) 21

[8] G. Provatas et al., Nucl. Instr. and Meth. in Phys. Res. B472 (2020) 36

[9] D. Gockel, Master Thesis, Kalibration der Ionenstrahlenergie des 4MV-Tandembeschleunigers am RUBION, Faculty of Physics and Astronomy, Ruhr University Bochum (2021)

[10] M. Mayer, Nucl. Instr. and Meth. in Phys. Res. B332 (2014) 176

[11] J. F. Ziegler, M. D. Ziegler, J. P. Biersack, Nucl. Instr. and Meth. in Phys. Res. B268 (2010), 1818

[12] E. Ntemou et al., Nucl. Instr. and Meth. in Phys. Res. B459 (2019) 90

[13] F. Machali et al., J. Atomkernenergie 13 (1968) 29

[14] J. H. Renken et al., Phys. Rev. 132 (1963) 2627

[15] I. Lombardo et al., Nucl. Instr. and Meth. in Phys. Res. B302 (2013) 19

[16] J. Liu et al., Nucl. Instr. and Meth. in Phys. Res. B108 (1996) 247

[17] J. A. Leavitt et al., Nucl. Instr. and Meth. in Phys. Res. B85 (1994) 37

[18] J. Theuerkauf, S. Esser, S. Krink, M. Luig, N. Nicolay, O. Stuch, H. Wolters, Program Tv, Institute for Nuclear Physics, Cologne (2007)

[19] Guide to the Expression of Uncertainty in Measurement, International Organization for Standardization, Geneva, Switzerland (1995) ISBN 92-67-10188-9

Table captions

Table 1. Statistical and systematic errors contributing to the total estimated uncertainty.

Table 2. Differential cross sections of the ^{9}Be(^{3}He, ^{3}He) ^{9}Be elastic scattering. The reported errors correspond to the total estimated uncertainty.

Table 3. Differential cross sections of the $^{9}Be(^{3}He, p_0)^{11}B$ reaction. The reported errors correspond to the total estimated uncertainty.

Table 4. Differential cross sections of the $^{9}Be(^{3}He, p_1)^{11}B$ reaction. The reported errors correspond to the total estimated uncertainty.

Table 5. Differential cross sections of the $^{9}Be(^{3}He, p_2)^{11}B$ reaction. The reported errors correspond to the total estimated uncertainty.

Table 6. Differential cross sections of the $^{9}Be(^{3}He, p_3)^{11}B$ reaction. The reported errors correspond to the total estimated uncertainty.

Table 7. Differential cross sections of the $^{9}Be(^{3}He, p_{4+5})^{11}B$ reaction. The reported errors correspond to the total estimated uncertainty.

Table 8. Differential cross sections of the $^{9}Be(^{3}He, p_6)^{11}B$ reaction. The reported errors correspond to the total estimated uncertainty.

Table 9. Differential cross sections of the $^{9}Be(^{3}He, p_7)^{11}B$ reaction. The reported errors correspond to the total estimated uncertainty.

Figure captions

Figure 1. Drawing of the experimental setup used at RUBION.

Figure 2. Typical experimental spectrum measured at E_{lab}=2518 keV and at 160°. Panel (a) corresponds to the high energy part of the spectrum, and panel (b) the low energy part.

Figure 3. Analysis of the thin Be target used in the differential cross-section measurements: (a) d-EBS at E_d=1785 keV and θ=160°. (b) α-EBS at E_α=3780 keV and θ=160°.

Figure 4. Differential cross–section values of the $^{9}Be(^{3}He,^{3}He_0)$ elastic scattering determined for the scattering angles of (a) 120º, (b) 130º, (c) 140º, (d) 150º, (e) 160º and (f) 170º. The present data are shown with black dots while the red triangles correspond to the data of Bondouk et al. [5] at 122°, 137° and 145°. In the energy ranges from about 3000 to about 4500 keV cross-section values could not be determined due to overlap of the $^{9}Be(^{3}He,^{3}He_0)$ elastic scattering signal with peaks from nuclear reactions. The error bars include only the statistical uncertainties resulting from the determination of the peak areas and the uncertainties in the N_{Au}/N_{Be} and N_{Cu}/N_{Be} thickness ratios.

Figure 5. Differential cross–section values of the $^{9}Be(^{3}He,p_0)^{11}B$ reaction at (a) 120º, (b) 130º, (c) 140º, (d) 150º, (e) 160º and (f) 170º. The black dots correspond to the data obtained in the present data while the red open squares, blue open triangles and green open dots to data from Wolicki et al. [6], Barradas et al. [7] and Provatas et al. [8], respectively. The error bars include only the statistical uncertainties resulting from the determination of the peak areas and the uncertainties in the N_{Au}/N_{Be} and N_{Cu}/N_{Be} thickness ratios.

Figure 6. Same as in Fig. 4 for the $^{9}Be(^{3}He,p_1)^{11}B$ reaction.

Figure 7. Differential cross sections of the $^{9}Be(^{3}He,p_2)^{11}B$ reaction for scattering angle (a) 120^o, (b) 130^o, (c) 140^o, (d) 150^o, (e) 160^o and (f) 170^o. The data obtained in this work are presented with black dots while the blue open triangles and green open dots correspond to data from Barradas et al. [7] and Provatas et al. [8], respectively. The error bars include only the statistical uncertainties resulting from the determination of the peak areas and the uncertainties in the N_{Au}/N_{Be} and N_{Cu}/N_{Be} thickness ratios.

Figure 8. Same as in Fig. 6 for the $^{9}Be(^{3}He,p_3)^{11}B$ reaction.

Figure 9. Differential cross–section values of the $^{9}Be(^{3}He,p_{4+5})^{11}B$ reaction at (a) 120^o, (b) 130^o, (c) 140^o, (d) 150^o, (e) 160^o and (f) 170^o. The current datasets are shown with black dots while the green open dots correspond to the data of Provatas et al. [8]. The error bars include only the statistical uncertainties resulting from the determination of the peak areas and the uncertainties in the N_{Au}/N_{Be} and N_{Cu}/N_{Be} thickness ratios.

Figure 10. Same as in Fig. 8 for the $^{9}Be(^{3}He,p_6)^{11}B$ reaction.

Figure 11. Differential cross–section values of the $^{9}Be(^{3}He,p_7)^{11}B$ reaction at (a) 120^o, (b) 130^o, (c) 140^o, (d) 150^o, (e) 160^o and (f) 170^o. According to the authors' best knowledge, there are no other data available in literature for this reaction. The error bars include only the statistical uncertainties resulting from the determination of the peak areas and the uncertainties in the N_{Au}/N_{Be} and N_{Cu}/N_{Be} thickness ratios.

Figure 12. Energy and angular variation of the obtained differential cross-section values for the (a) $^{9}Be(^{3}He,^{3}He_{0})$ elastic scattering, and (b) $^{9}Be(^{3}He,p_{0})^{11}B$, (c) $^{9}Be(^{3}He,p_{1})^{11}B$, (d) $^{9}Be(^{3}He,p_{2})^{11}B$, (e) $^{9}Be(^{3}He,p_{3})^{11}B$, (f) $^{9}Be(^{3}He,p_{4+5})^{11}B$, (g) $^{9}Be(^{3}He,p_{6})^{11}B$ (h) $^{9}Be(^{3}He,p_{7})^{11}B$ reactions. The error bars include only the statistical uncertainties resulting from the determination of the peak areas and the uncertainties in the N_{Au}/N_{Be} and N_{Cu}/N_{Be} thickness ratios.

Figure 13. Experimental and simulated benchmarking spectra obtained at RUBION, Bochum (panels a, c, e, f, g, h, i), and at RBI, Zagreb (panels b, d).

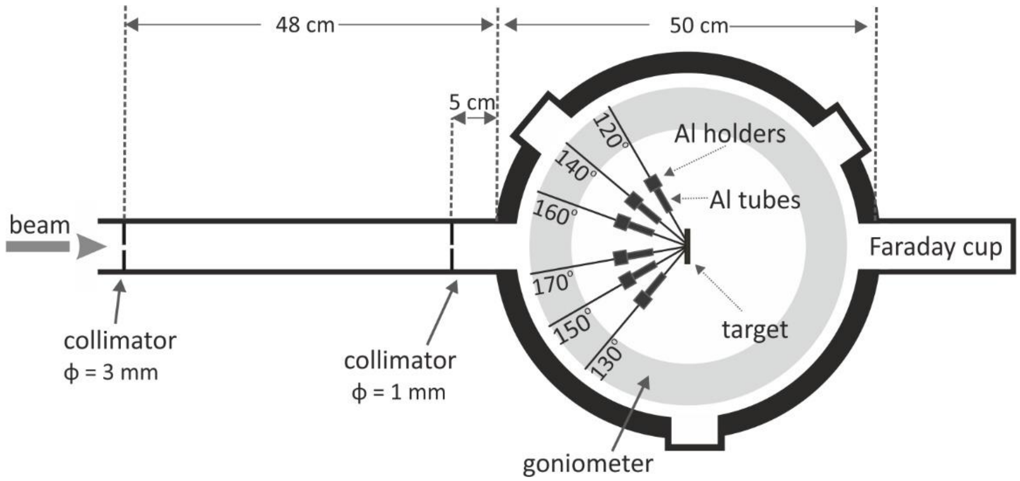
48 cm
50 cm
5 cm
beam
120°
140°
160°
170°
150°
130°
Al holders
Al tubes
Faraday cup
target
collimator
ϕ = 3 mm
collimator
ϕ = 1 mm
goniometer

Figure 1

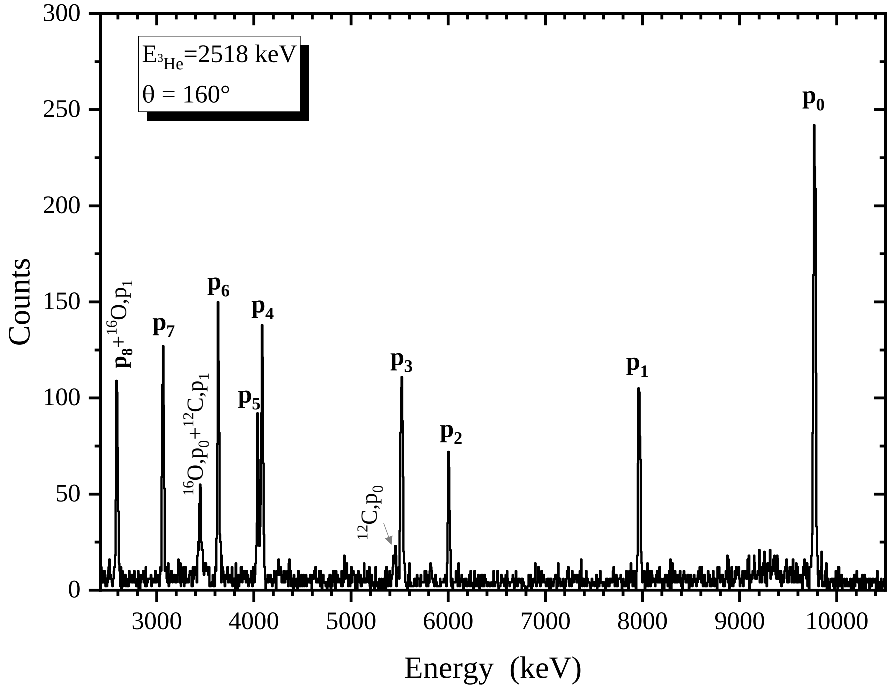
E3He=2518 keV
θ = 160°
Counts
Energy (keV)
p0
p1
p2
p3
p4
p5
p6
p7
p8+16O,p1
16O,p0+12C,p1
12C,p0

Figure 2a

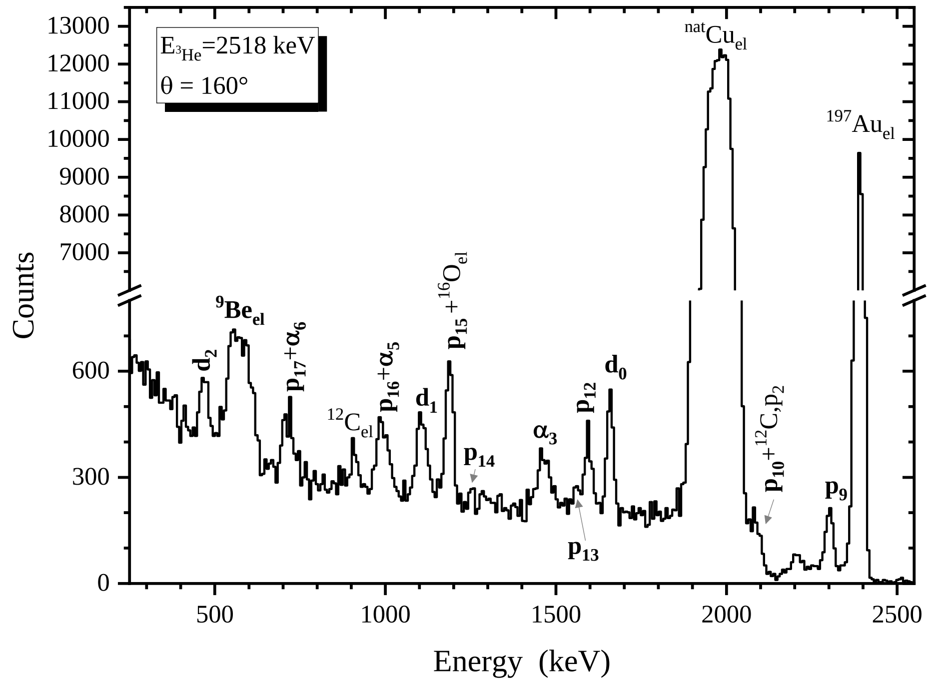

E3He=2518 keV
θ = 160°
natCuel
197Auel
9Beel
d2
p17+α6
12Cel
p16+α5
d1
p15 +16Oel
p14
α3
p12
d0
p13
p10+12C,p2
p9
Counts
Energy (keV)

Figure 2b

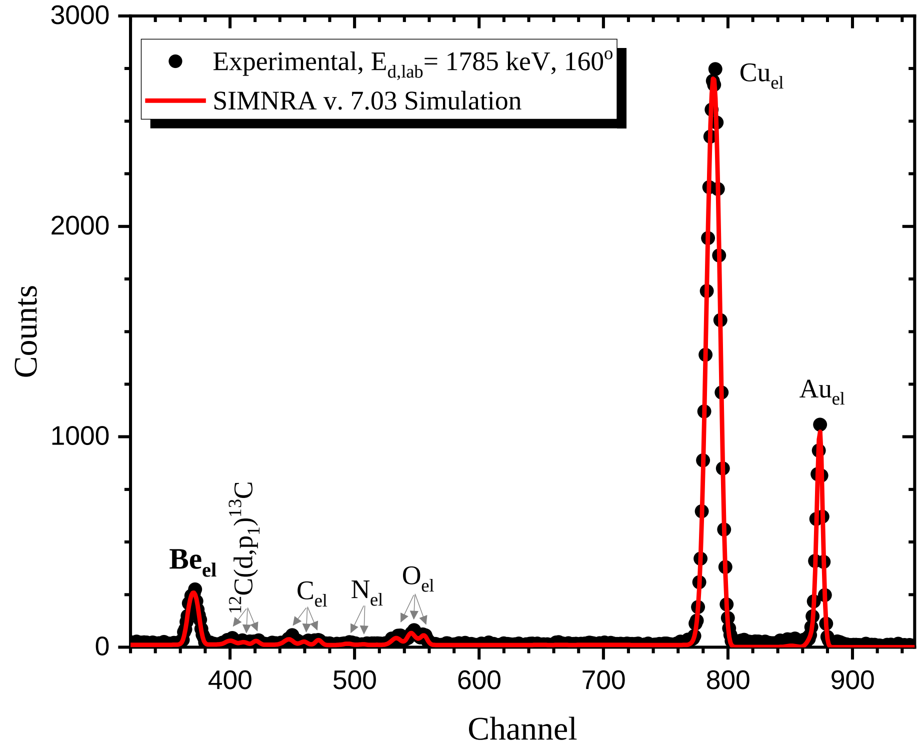

3000
2000
1000
0
Counts
400
500
600
700
800
900
Channel
Experimental, $E_{d,lab}$= 1785 keV, 160^o
SIMNRA v. 7.03 Simulation
Cu_{el}
Au_{el}
$\mathbf{Be_{el}}$
$^{12}C(d,p_1)^{13}C$
C_{el}
N_{el}
O_{el}

Figure 3a

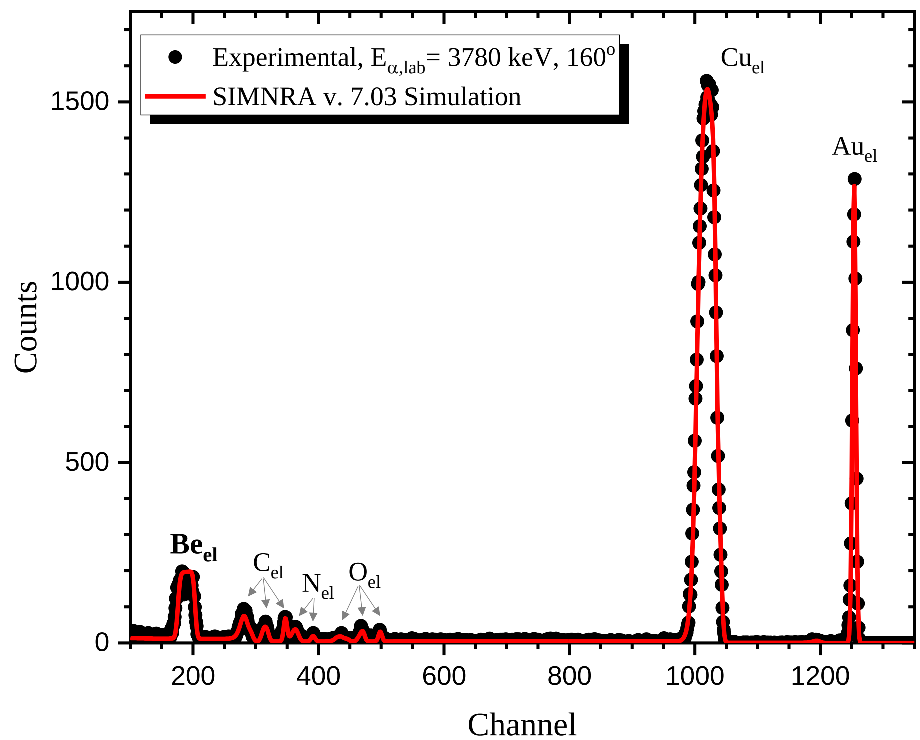

Experimental, E$_{\alpha,lab}$= 3780 keV, 160^o
SIMNRA v. 7.03 Simulation
Cu$_{el}$
Au$_{el}$
Be$_{el}$
C$_{el}$
N$_{el}$
O$_{el}$
Counts
Channel
0
500
1000
1500
200
400
600
800
1000
1200

Figure 3b

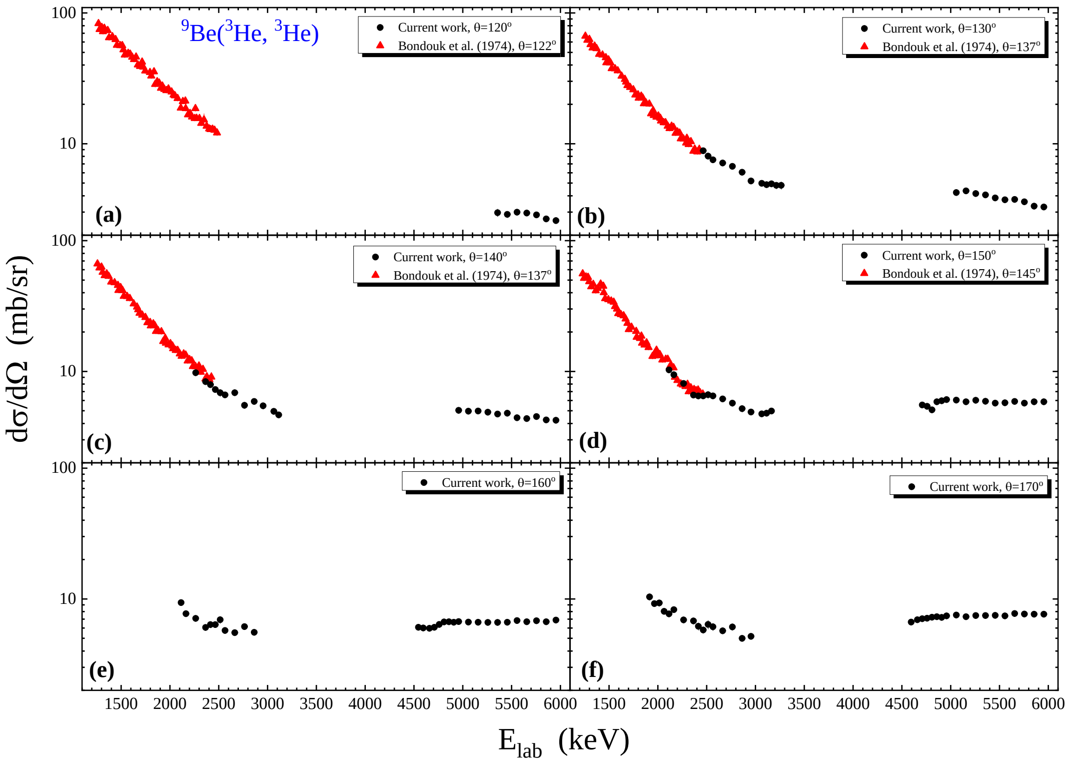

$^{9}Be(^{3}He, ^{3}He)$
Current work, θ=120°
Bondouk et al. (1974), θ=122°
Current work, θ=130°
Bondouk et al. (1974), θ=137°
Current work, θ=140°
Bondouk et al. (1974), θ=137°
Current work, θ=150°
Bondouk et al. (1974), θ=145°
Current work, θ=160°
Current work, θ=170°
(a)
(b)
(c)
(d)
(e)
(f)
dσ/dΩ (mb/sr)
E_{lab} (keV)

Figure 4

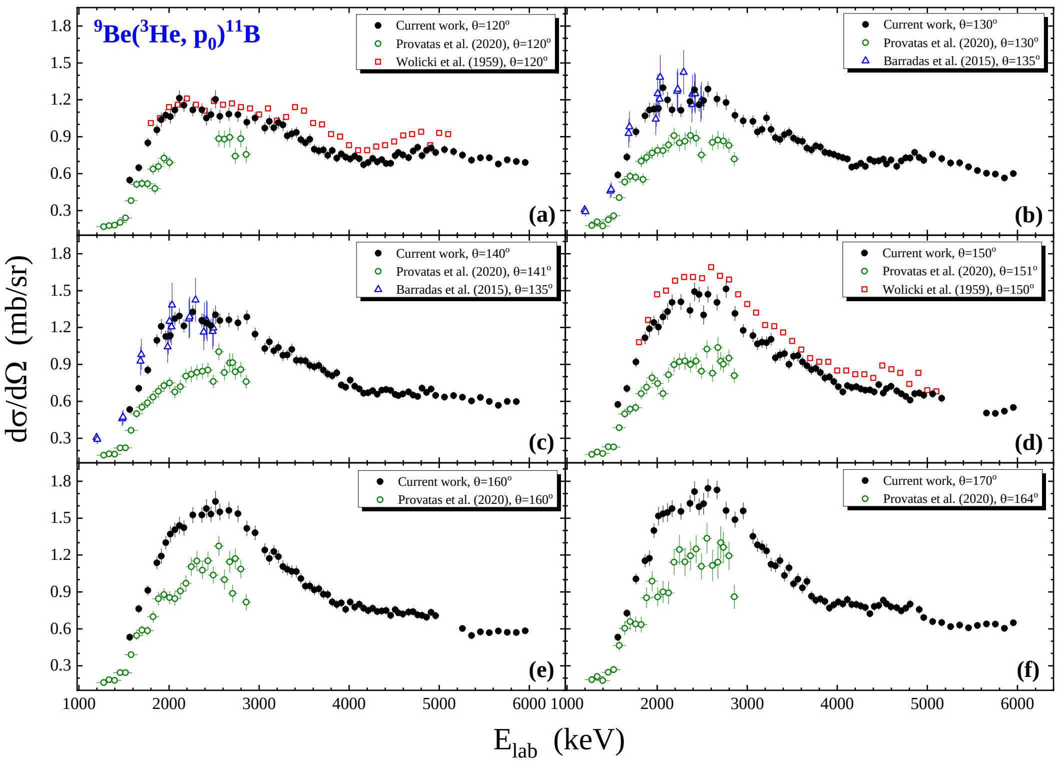

^{9}Be(^{3}He, p$_0$)^{11}B
Current work, θ=120°
Provatas et al. (2020), θ=120°
Wolicki et al. (1959), θ=120°
(a)
Current work, θ=130°
Provatas et al. (2020), θ=130°
Barradas et al. (2015), θ=135°
(b)
Current work, θ=140°
Provatas et al. (2020), θ=141°
Barradas et al. (2015), θ=135°
(c)
Current work, θ=150°
Provatas et al. (2020), θ=151°
Wolicki et al. (1959), θ=150°
(d)
Current work, θ=160°
Provatas et al. (2020), θ=160°
(e)
Current work, θ=170°
Provatas et al. (2020), θ=164°
(f)
dσ/dΩ (mb/sr)
E$_{lab}$ (keV)

Figure 5

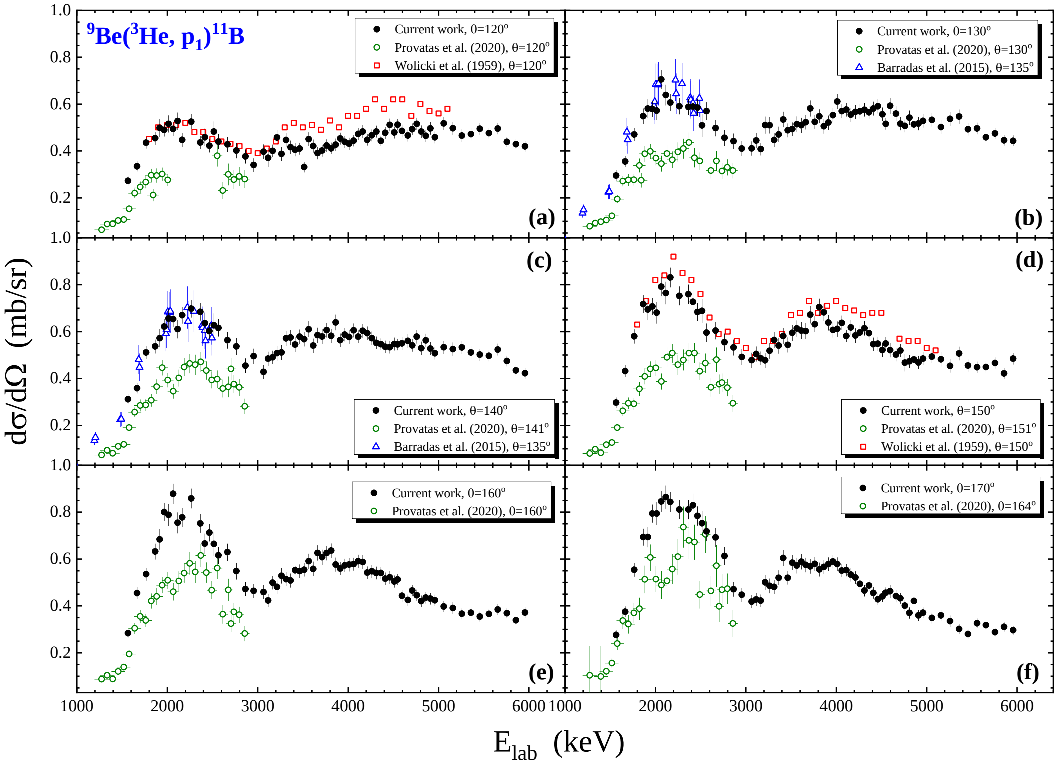

$^9Be(^3He, p_1)^{11}B$
Current work, θ=120°
Provatas et al. (2020), θ=120°
Wolicki et al. (1959), θ=120°
Current work, θ=130°
Provatas et al. (2020), θ=130°
Barradas et al. (2015), θ=135°
Current work, θ=140°
Provatas et al. (2020), θ=141°
Barradas et al. (2015), θ=135°
Current work, θ=150°
Provatas et al. (2020), θ=151°
Wolicki et al. (1959), θ=150°
Current work, θ=160°
Provatas et al. (2020), θ=160°
Current work, θ=170°
Provatas et al. (2020), θ=164°
(a)
(b)
(c)
(d)
(e)
(f)
dσ/dΩ (mb/sr)
E_{lab} (keV)

Figure 6

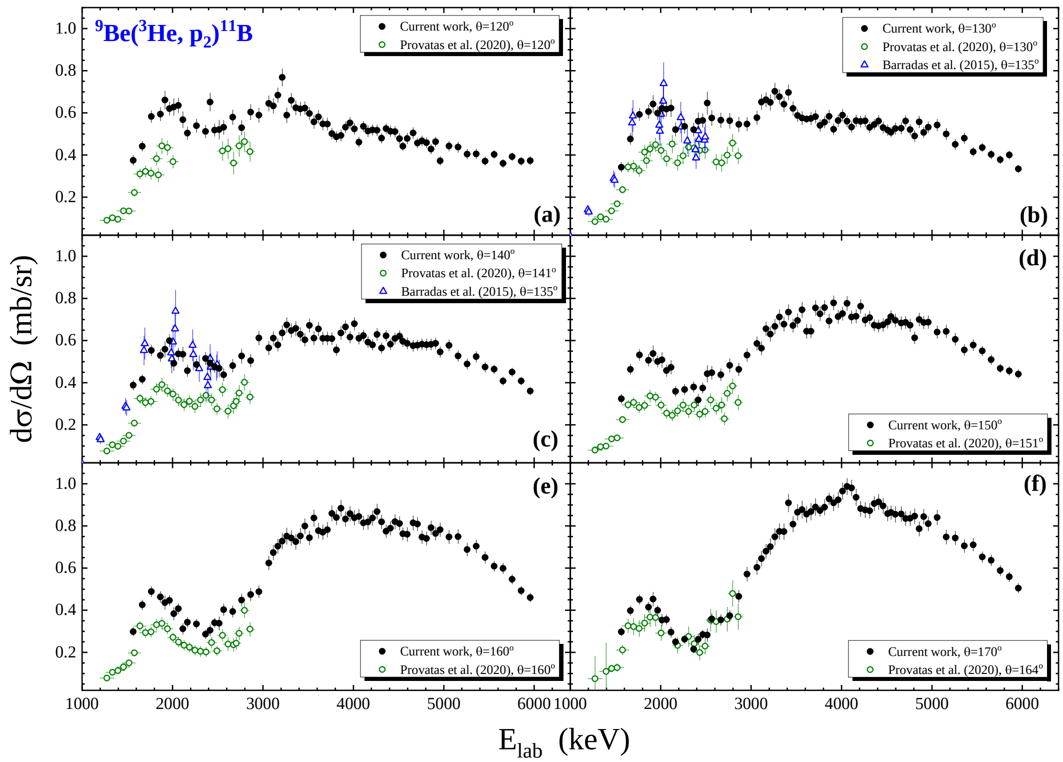

$^{9}Be(^{3}He, p_2)^{11}B$
Current work, θ=120°
Provatas et al. (2020), θ=120°
Current work, θ=130°
Provatas et al. (2020), θ=130°
Barradas et al. (2015), θ=135°
Current work, θ=140°
Provatas et al. (2020), θ=141°
Barradas et al. (2015), θ=135°
Current work, θ=150°
Provatas et al. (2020), θ=151°
Current work, θ=160°
Provatas et al. (2020), θ=160°
Current work, θ=170°
Provatas et al. (2020), θ=164°
(a)
(b)
(c)
(d)
(e)
(f)
dσ/dΩ (mb/sr)
E_{lab} (keV)

Figure 7

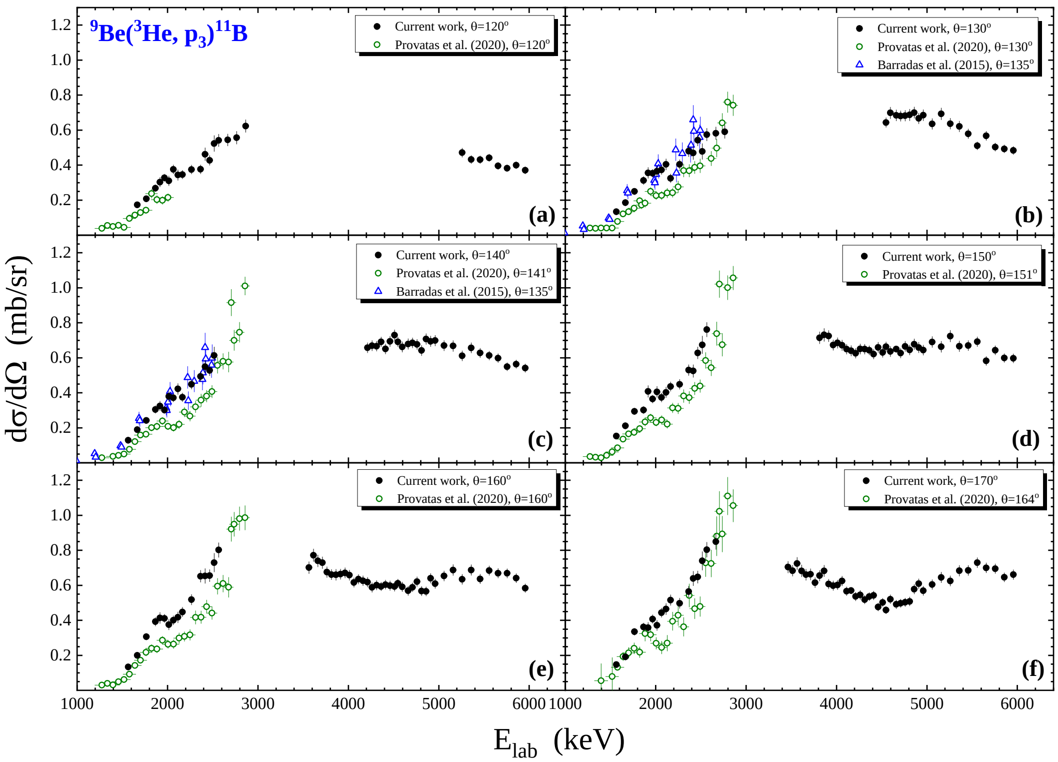

$^9Be(^3He, p_3)^{11}B$
Current work, θ=120°
Provatas et al. (2020), θ=120°
Current work, θ=130°
Provatas et al. (2020), θ=130°
Barradas et al. (2015), θ=135°
Current work, θ=140°
Provatas et al. (2020), θ=141°
Barradas et al. (2015), θ=135°
Current work, θ=150°
Provatas et al. (2020), θ=151°
Current work, θ=160°
Provatas et al. (2020), θ=160°
Current work, θ=170°
Provatas et al. (2020), θ=164°
(a)
(b)
(c)
(d)
(e)
(f)
dσ/dΩ (mb/sr)
E_{lab} (keV)

Figure 8

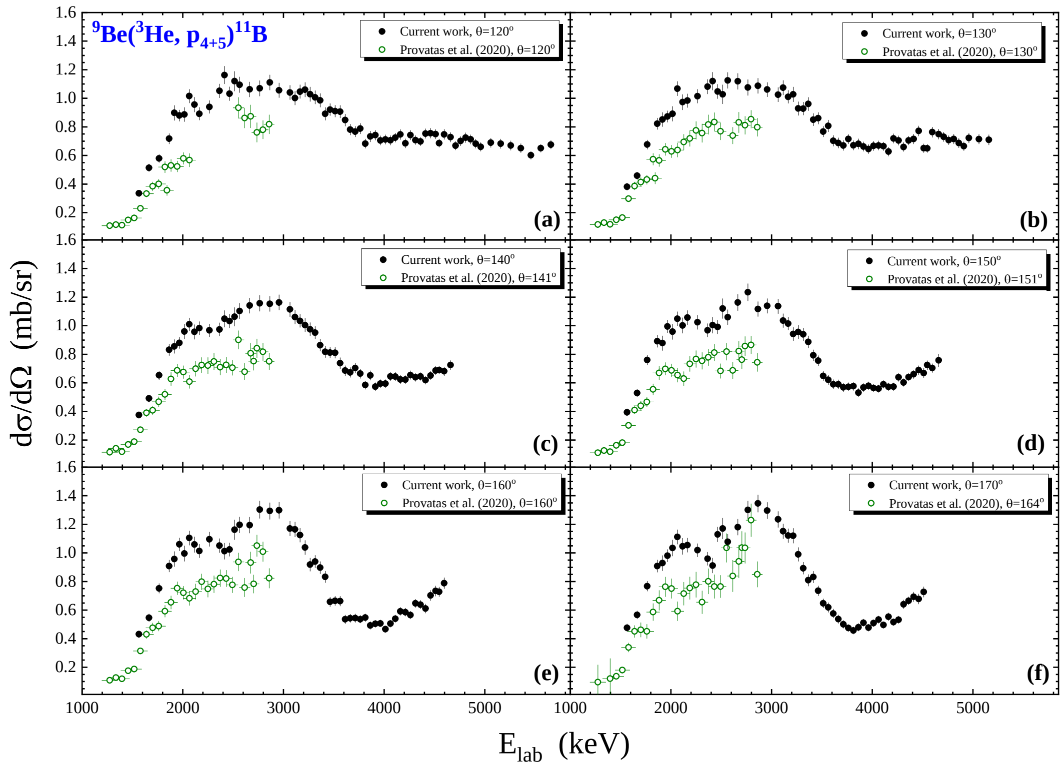

$^{9}Be(^{3}He, p_{4+5})^{11}B$
Current work, θ=120°
Provatas et al. (2020), θ=120°
(a)
Current work, θ=130°
Provatas et al. (2020), θ=130°
(b)
Current work, θ=140°
Provatas et al. (2020), θ=141°
(c)
Current work, θ=150°
Provatas et al. (2020), θ=151°
(d)
Current work, θ=160°
Provatas et al. (2020), θ=160°
(e)
Current work, θ=170°
Provatas et al. (2020), θ=164°
(f)
dσ/dΩ (mb/sr)
E_{lab} (keV)

Figure 9

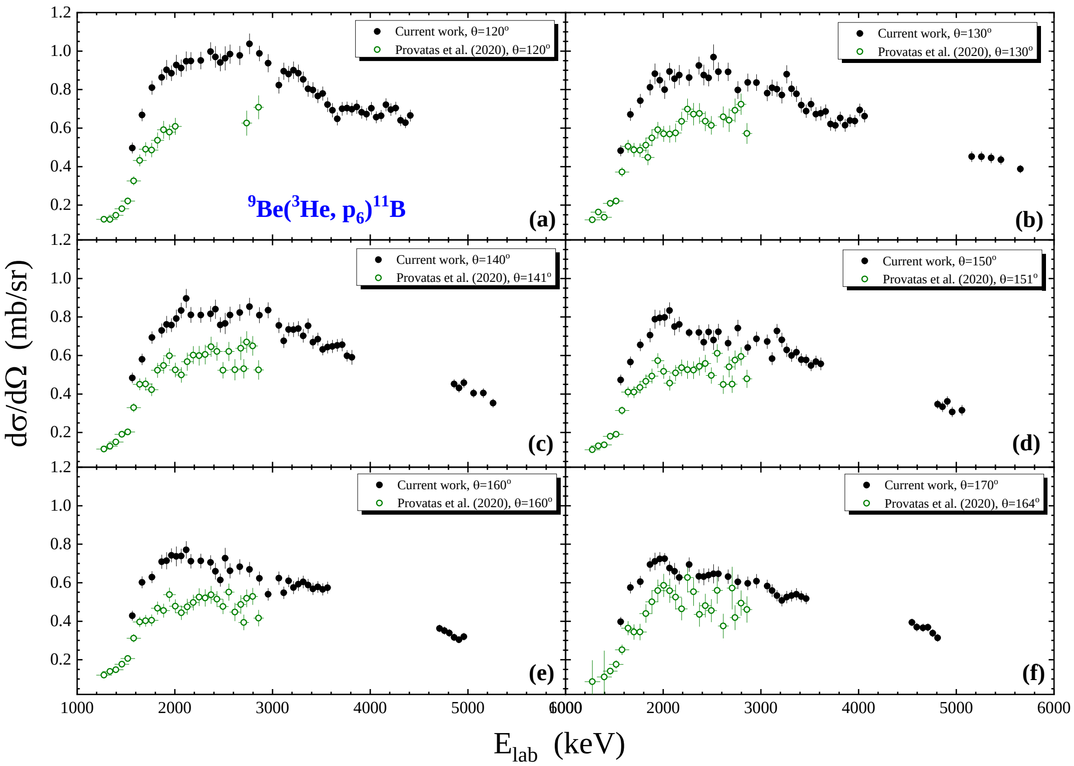

Current work, θ=120°
Provatas et al. (2020), θ=120°
^{9}Be(^{3}He, p$_6$)^{11}B
(a)
Current work, θ=130°
Provatas et al. (2020), θ=130°
(b)
Current work, θ=140°
Provatas et al. (2020), θ=141°
(c)
Current work, θ=150°
Provatas et al. (2020), θ=151°
(d)
Current work, θ=160°
Provatas et al. (2020), θ=160°
(e)
Current work, θ=170°
Provatas et al. (2020), θ=164°
(f)
dσ/dΩ (mb/sr)
E$_{lab}$ (keV)

Figure 10

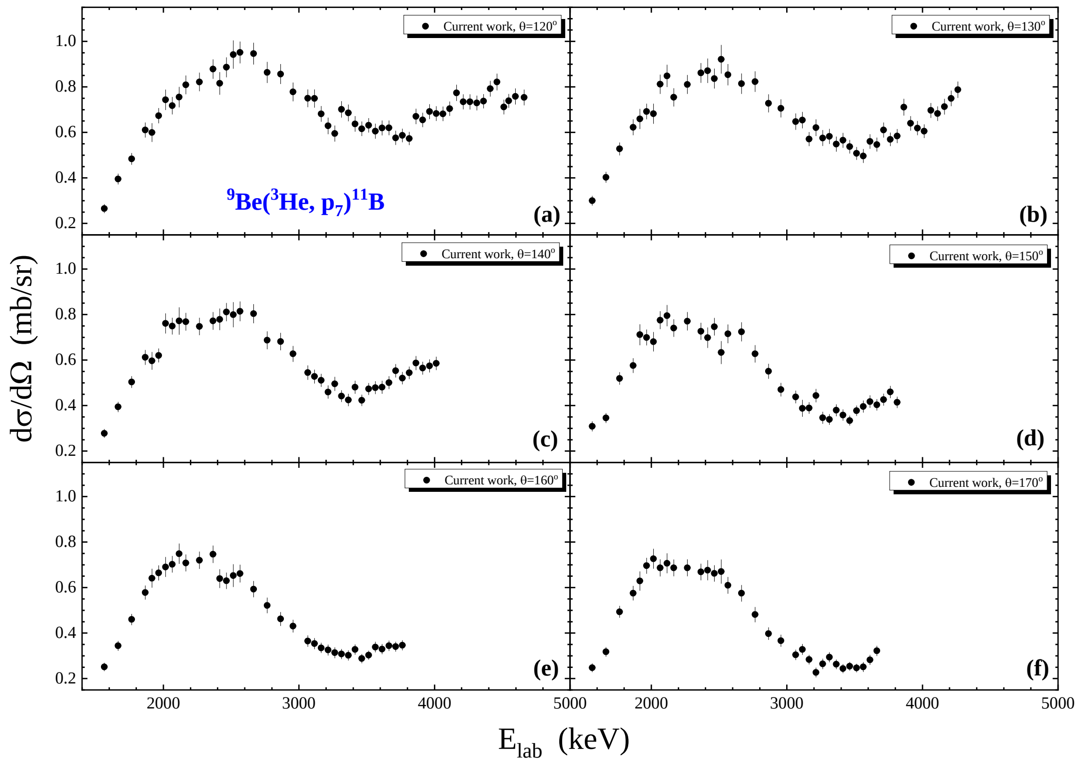
Current work, θ=120°
Current work, θ=130°
Current work, θ=140°
Current work, θ=150°
Current work, θ=160°
Current work, θ=170°
⁹Be(³He, p₇)¹¹B
(a)
(b)
(c)
(d)
(e)
(f)
dσ/dΩ (mb/sr)
E_lab (keV)

Figure 11

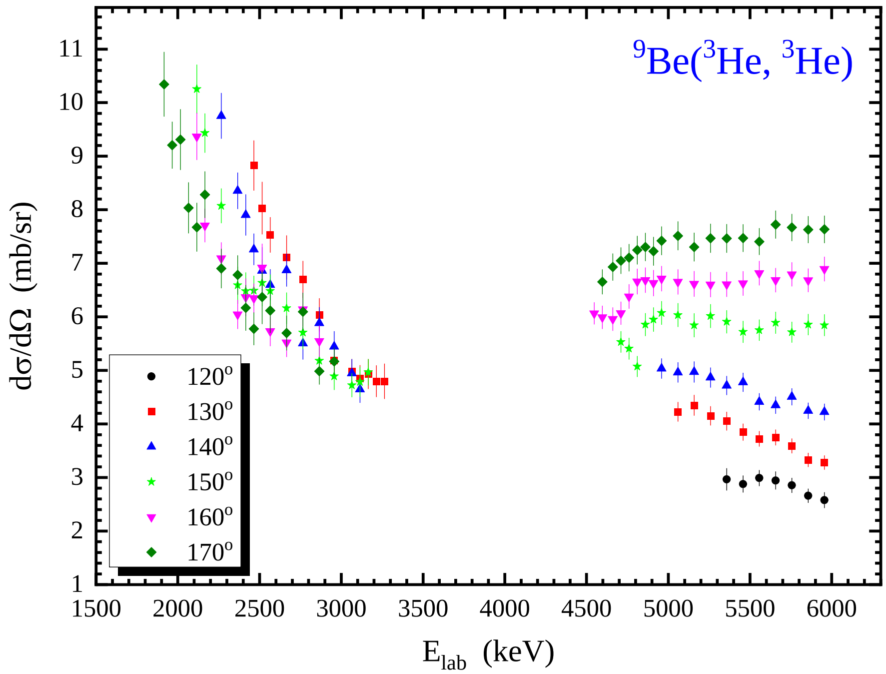

$^{9}Be(^{3}He, ^{3}He)$
$d\sigma/d\Omega$ (mb/sr)
E_{lab} (keV)
120°
130°
140°
150°
160°
170°

Figure 12a

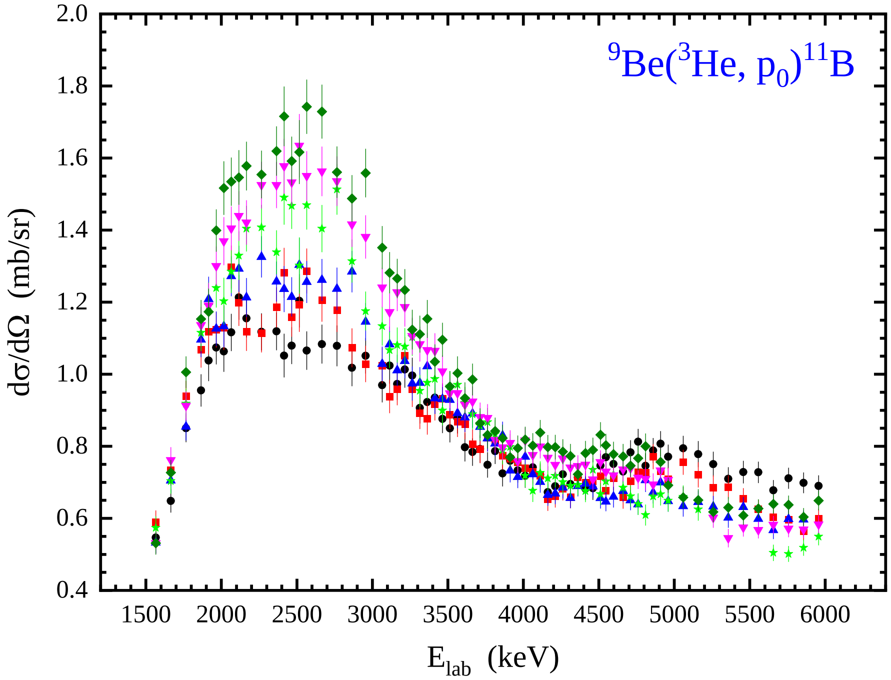

^{9}Be(^{3}He, p_0)^{11}B
dσ/dΩ (mb/sr)
E_{lab} (keV)
2.0
1.8
1.6
1.4
1.2
1.0
0.8
0.6
0.4
1500
2000
2500
3000
3500
4000
4500
5000
5500
6000

Figure 12b

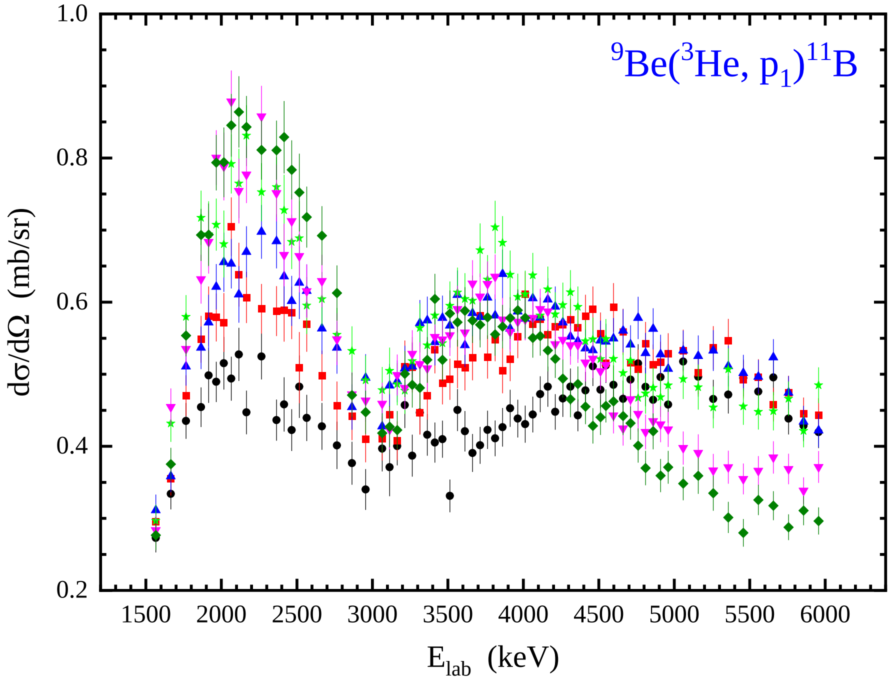

$^{9}Be(^{3}He, p_{1})^{11}B$
1.0
0.8
0.6
0.4
0.2
dσ/dΩ (mb/sr)
1500
2000
2500
3000
3500
4000
4500
5000
5500
6000
E_{lab} (keV)

Figure 12c

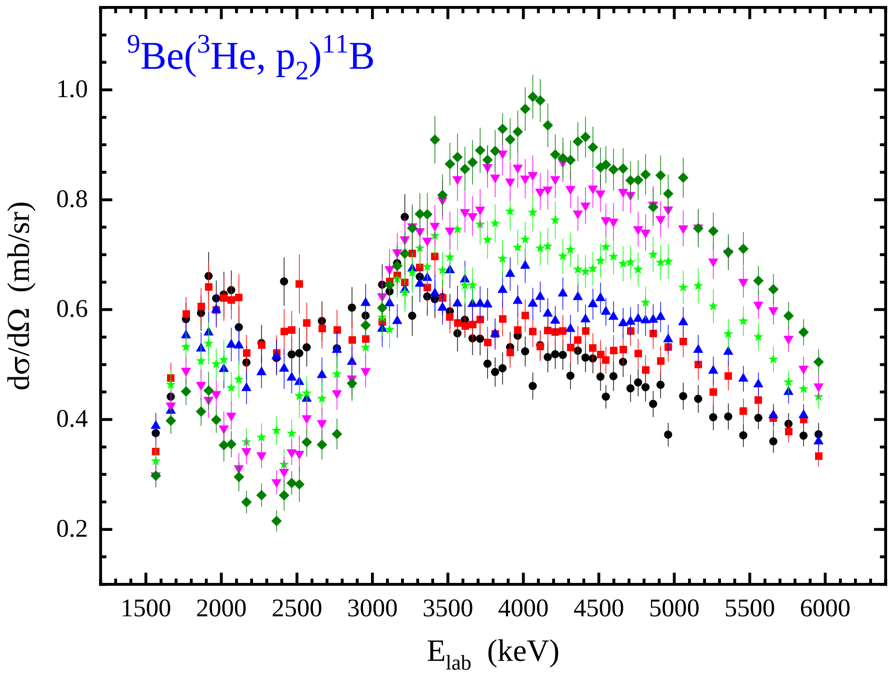
^{9}Be(^{3}He, p_2)^{11}B
dσ/dΩ (mb/sr)
0.2
0.4
0.6
0.8
1.0
1500
2000
2500
3000
3500
4000
4500
5000
5500
6000
E_{lab} (keV)

Figure 12d

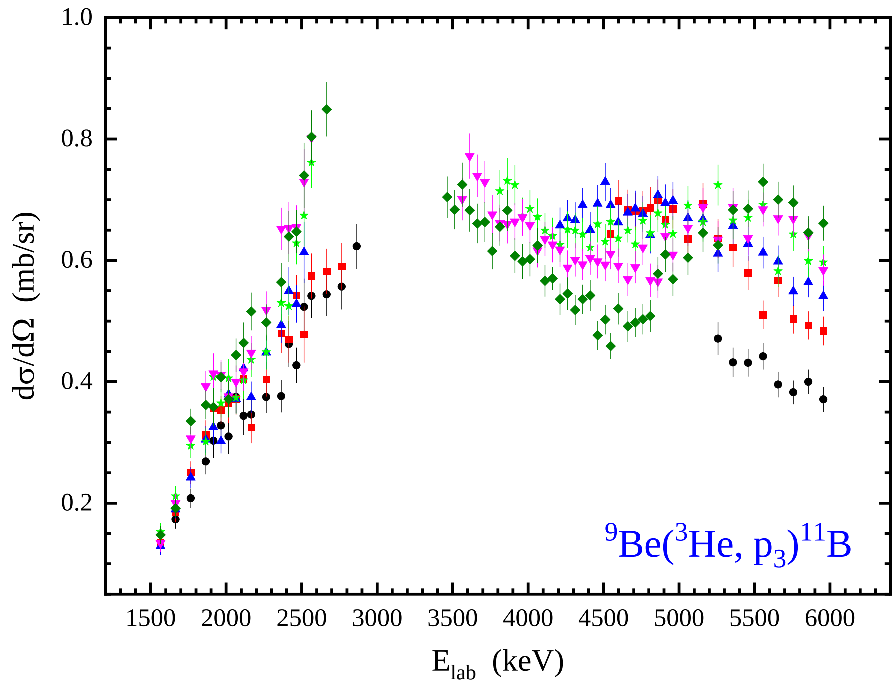

1.0
0.8
0.6
0.4
0.2
dσ/dΩ (mb/sr)
1500
2000
2500
3000
3500
4000
4500
5000
5500
6000
E_{lab} (keV)
$^{9}Be(^{3}He, p_{3})^{11}B$

Figure 12e

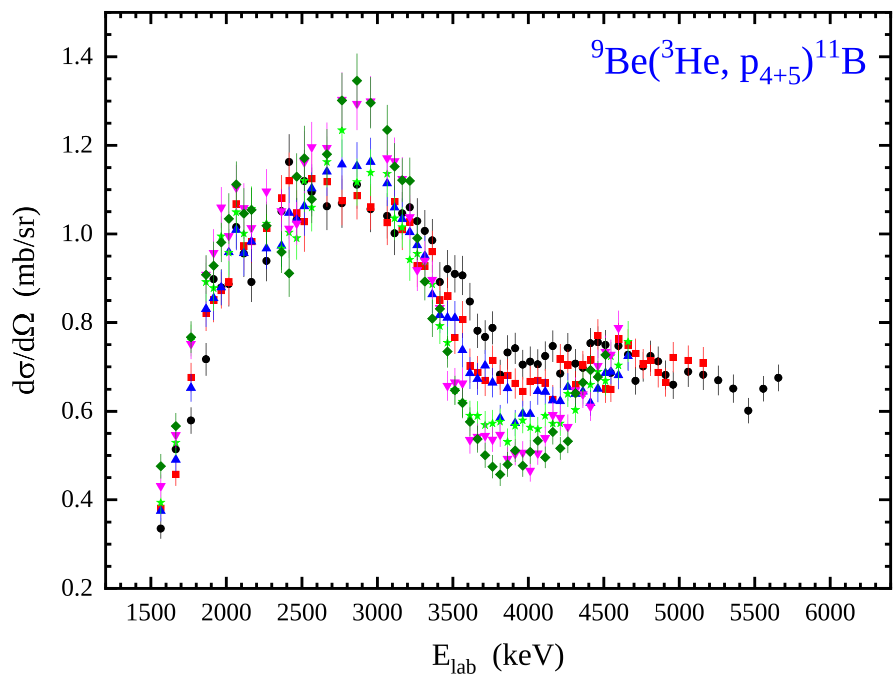
$^{9}Be(^{3}He, p_{4+5})^{11}B$
1.4
1.2
1.0
0.8
0.6
0.4
0.2
dσ/dΩ (mb/sr)
1500
2000
2500
3000
3500
4000
4500
5000
5500
6000
E_{lab} (keV)

Figure 12f

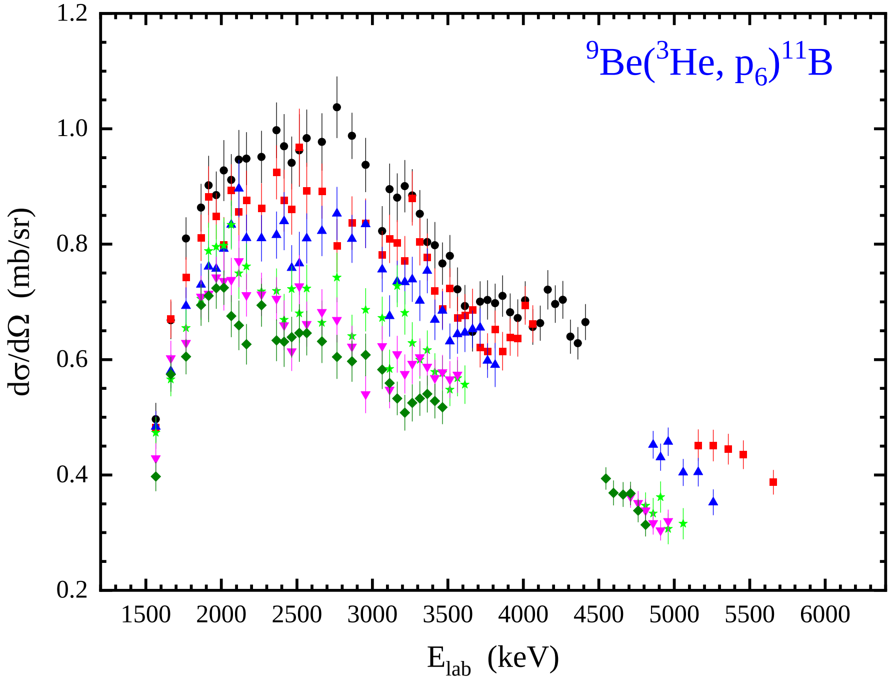

$^{9}Be(^{3}He, p_6)^{11}B$
dσ/dΩ (mb/sr)
E_{lab} (keV)
1.2
1.0
0.8
0.6
0.4
0.2
1500
2000
2500
3000
3500
4000
4500
5000
5500
6000

Figure 12g

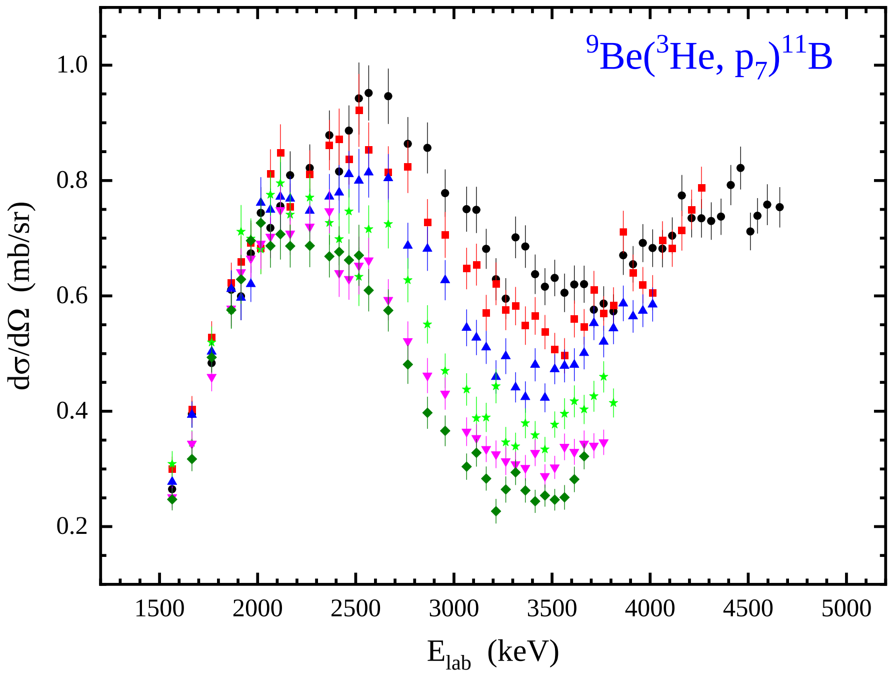

$^{9}Be(^{3}He, p_{7})^{11}B$
1.0
0.8
0.6
0.4
0.2
dσ/dΩ (mb/sr)
1500
2000
2500
3000
3500
4000
4500
5000
E_{lab} (keV)

Figure 12h

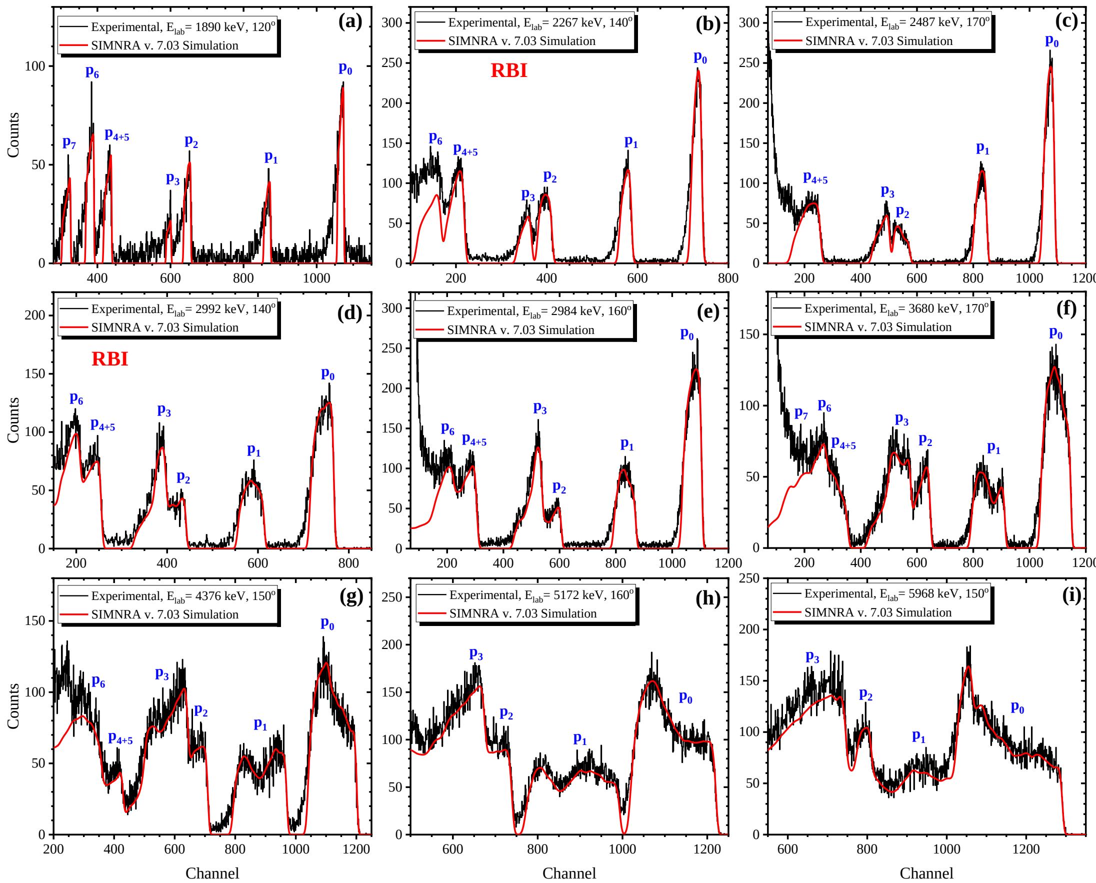
Experimental, E_lab= 1890 keV, 120°
SIMNRA v. 7.03 Simulation
(a)
Experimental, E_lab= 2267 keV, 140°
SIMNRA v. 7.03 Simulation
(b)
RBI
Experimental, E_lab= 2487 keV, 170°
SIMNRA v. 7.03 Simulation
(c)
Experimental, E_lab= 2992 keV, 140°
SIMNRA v. 7.03 Simulation
(d)
RBI
Experimental, E_lab= 2984 keV, 160°
SIMNRA v. 7.03 Simulation
(e)
Experimental, E_lab= 3680 keV, 170°
SIMNRA v. 7.03 Simulation
(f)
Experimental, E_lab= 4376 keV, 150°
SIMNRA v. 7.03 Simulation
(g)
Experimental, E_lab= 5172 keV, 160°
SIMNRA v. 7.03 Simulation
(h)
Experimental, E_lab= 5968 keV, 150°
SIMNRA v. 7.03 Simulation
(i)
Counts
Channel

Figure 13

Reaction	$\frac{N_{Au}}{N_{Be}}$	$\frac{N_{Cu}}{N_{Be}}$	Target homogeneity	Peak integration	Total estimated uncertainty
	(%)				
^{9}Be(^{3}He,^{3}He$_0$)^{9}Be	3.6	3.4	3	1.3 – 7.3	4.9 – 8.7
^{9}Be(^{3}He,p$_0$)^{11}B				2.6 – 5.5	5.3 – 7.2
^{9}Be(^{3}He,p$_1$)^{11}B				3.1 – 10.4	5.6 – 11.4
^{9}Be(^{3}He,p$_2$)^{11}B				2.5 – 10.8	5.3 – 11.8
^{9}Be(^{3}He,p$_3$)^{11}B				2.7 – 10.9	5.4 – 11.9
^{9}Be(^{3}He,p$_{4+5}$)^{11}B				2.8 – 6.1	5.4 – 7.7
^{9}Be(^{3}He,p$_6$)^{11}B				2.7 – 8.1	5.4 – 9.4
^{9}Be(^{3}He,p$_7$)^{11}B				2.8 – 9.1	5.5 – 10.2

Table 1

E_{lab} (keV)	dσ/dΩ (mb/sr)					
	120°	130°	140°	150°	160°	170°
1916 ± 3	-	-	-	-	-	10.3 ± 0.7
1966 ± 3	-	-	-	-	-	9.2 ± 0.5
2016 ± 3	-	-	-	-	-	9.3 ± 0.7
2066 ± 3	-	-	-	-	-	8.0 ± 0.6
2116 ± 3	-	-	-	10.3 ± 0.6	9.4 ± 0.6	7.7 ± 0.5
2166 ± 3	-	-	-	9.4 ± 0.5	7.7 ± 0.4	8.3 ± 0.5
2266 ± 3	-	-	9.8 ± 0.5	8.1 ± 0.4	7.1 ± 0.4	6.9 ± 0.4
2366 ± 3	-	-	8.4 ± 0.5	6.6 ± 0.4	6.0 ± 0.3	6.8 ± 0.4
2416 ± 3	-	-	7.9 ± 0.5	6.5 ± 0.4	6.4 ± 0.4	6.2 ± 0.5
2466 ± 3	-	8.8 ± 0.6	7.3 ± 0.4	6.5 ± 0.4	6.3 ± 0.4	5.8 ± 0.4
2516 ± 3	-	8.0 ± 0.6	6.9 ± 0.5	6.6 ± 0.5	6.9 ± 0.5	6.4 ± 0.6
2566 ± 3	-	7.5 ± 0.4	6.6 ± 0.4	6.5 ± 0.4	5.7 ± 0.3	6.1 ± 0.5
2666 ± 3	-	7.1 ± 0.5	6.9 ± 0.4	6.2 ± 0.4	5.5 ± 0.3	5.7 ± 0.4
2765 ± 3	-	6.7 ± 0.4	5.5 ± 0.4	5.7 ± 0.4	6.1 ± 0.4	6.1 ± 0.4
2865 ± 3	-	6.0 ± 0.4	5.9 ± 0.4	5.2 ± 0.3	5.5 ± 0.4	5.0 ± 0.3
2956 ± 3	-	5.9 ± 0.3	5.4 ± 0.3	4.9 ± 0.3	-	5.2 ± 0.3
3065 ± 3	-	4.98 ± 0.29	4.9 ± 0.3	4.72 ± 0.28	-	-
3115 ± 3	-	4.9 ± 0.3	4.6 ± 0.3	4.8 ± 0.3	-	-
3165 ± 3	-	4.9 ± 0.3	-	5.0 ± 0.3	-	-
3215 ± 3	-	4.8 ± 0.3	-	-	-	-
3265 ± 3	-	4.8 ± 0.4	-	-	-	-
4547 ± 3	-	-	-	-	6.1 ± 0.3	-
4597 ± 3	-	-	-	-	6.0 ± 0.3	6.7 ± 0.3
4661 ± 3	-	-	-	-	6.0 ± 0.3	6.9 ± 0.4
4710 ± 3	-	-	-	5.53 ± 0.28	6.1 ± 0.3	7.0 ± 0.4
4760 ± 3	-	-	-	5.41 ± 0.28	6.4 ± 0.3	7.1 ± 0.4
4810 ± 3	-	-	-	5.07 ± 0.27	6.7 ± 0.3	7.2 ± 0.4
4860 ± 3	-	-	-	5.9 ± 0.3	6.7 ± 0.3	7.3 ± 0.4
4910 ± 3	-	-	-	6.0 ± 0.3	6.6 ± 0.3	7.2 ± 0.4
4960 ± 3	-	-	5.04 ± 0.26	6.1 ± 0.3	6.7 ± 0.3	7.4 ± 0.4
5059 ± 3	-	4.23 ± 0.24	4.96 ± 0.26	6.0 ± 0.3	6.7 ± 0.3	7.5 ± 0.4
5159 ± 3	-	4.35 ± 0.25	4.97 ± 0.26	5.8 ± 0.3	6.6 ± 0.3	7.3 ± 0.4
5258 ± 3	-	4.15 ± 0.23	4.87 ± 0.26	6.0 ± 0.3	6.6 ± 0.3	7.5 ± 0.4
5358 ± 3	2.97 ± 0.23	4.05 ± 0.23	4.72 ± 0.25	5.9 ± 0.3	6.6 ± 0.3	7.5 ± 0.4
5458 ± 3	2.88 ± 0.19	3.85 ± 0.21	4.78 ± 0.25	5.72 ± 0.29	6.6 ± 0.3	7.5 ± 0.4
5557 ± 3	2.99 ± 0.18	3.72 ± 0.20	4.41 ± 0.22	5.75 ± 0.28	6.8 ± 0.3	7.4 ± 0.4
5657 ± 3	2.94 ± 0.20	3.75 ± 0.20	4.35 ± 0.22	5.89 ± 0.29	6.7 ± 0.3	7.7 ± 0.4
5756 ± 3	2.85 ± 0.17	3.59 ± 0.19	4.51 ± 0.23	5.71 ± 0.28	6.8 ± 0.3	7.7 ± 0.4
5856 ± 3	2.66 ± 0.16	3.33 ± 0.18	4.25 ± 0.21	5.85 ± 0.29	6.7 ± 0.3	7.6 ± 0.4
5956 ± 3	2.58 ± 0.17	3.28 ± 0.18	4.22 ± 0.22	5.84 ± 0.29	6.9 ± 0.3	7.6 ± 0.4

Table 2

E_{lab} (keV)	dσ/dΩ (mb/sr)					
	120°	130°	140°	150°	160°	170°
1565 ± 3	0.55 ± 0.04	0.59 ± 0.04	0.53 ± 0.04	0.57 ± 0.04	0.53 ± 0.04	0.53 ± 0.04
1665 ± 3	0.65 ± 0.04	0.73 ± 0.04	0.71 ± 0.04	0.70 ± 0.04	0.76 ± 0.04	0.73 ± 0.04
1766 ± 3	0.85 ± 0.05	0.94 ± 0.05	0.85 ± 0.05	0.92 ± 0.05	0.91 ± 0.05	1.01 ± 0.06
1866 ± 3	0.95 ± 0.06	1.07 ± 0.06	1.10 ± 0.06	1.12 ± 0.06	1.14 ± 0.06	1.15 ± 0.07
1916 ± 3	1.04 ± 0.07	1.12 ± 0.07	1.21 ± 0.08	1.19 ± 0.08	1.19 ± 0.08	1.17 ± 0.08
1966 ± 3	1.07 ± 0.06	1.12 ± 0.06	1.13 ± 0.06	1.24 ± 0.07	1.30 ± 0.07	1.40 ± 0.08
2016 ± 3	1.06 ± 0.07	1.13 ± 0.07	1.13 ± 0.07	1.20 ± 0.08	1.37 ± 0.08	1.52 ± 0.09
2066 ± 3	1.12 ± 0.07	1.30 ± 0.08	1.27 ± 0.07	1.28 ± 0.07	1.40 ± 0.08	1.53 ± 0.09
2116 ± 3	1.21 ± 0.08	1.20 ± 0.08	1.29 ± 0.08	1.33 ± 0.08	1.44 ± 0.09	1.55 ± 0.09
2166 ± 3	1.16 ± 0.07	1.12 ± 0.07	1.21 ± 0.07	1.40 ± 0.08	1.42 ± 0.08	1.58 ± 0.09
2266 ± 3	1.12 ± 0.06	1.11 ± 0.07	1.33 ± 0.07	1.41 ± 0.08	1.52 ± 0.08	1.55 ± 0.09
2366 ± 3	1.12 ± 0.07	1.19 ± 0.07	1.26 ± 0.07	1.34 ± 0.08	1.53 ± 0.08	1.62 ± 0.09
2416 ± 3	1.05 ± 0.07	1.28 ± 0.08	1.24 ± 0.08	1.49 ± 0.09	1.58 ± 0.09	1.72 ± 0.10
2466 ± 3	1.08 ± 0.06	1.16 ± 0.07	1.21 ± 0.07	1.47 ± 0.08	1.53 ± 0.08	1.59 ± 0.09
2516 ± 3	1.20 ± 0.09	1.19 ± 0.09	1.30 ± 0.09	1.30 ± 0.09	1.63 ± 0.11	1.62 ± 0.11
2566 ± 3	1.07 ± 0.07	1.29 ± 0.08	1.26 ± 0.07	1.47 ± 0.09	1.55 ± 0.09	1.74 ± 0.10
2666 ± 3	1.08 ± 0.07	1.21 ± 0.07	1.26 ± 0.07	1.40 ± 0.08	1.56 ± 0.09	1.73 ± 0.10
2765 ± 3	1.08 ± 0.07	1.18 ± 0.07	1.24 ± 0.07	1.51 ± 0.09	1.54 ± 0.09	1.56 ± 0.09
2865 ± 3	1.02 ± 0.06	1.07 ± 0.07	1.28 ± 0.07	1.31 ± 0.08	1.42 ± 0.08	1.49 ± 0.08
2956 ± 3	1.05 ± 0.06	1.03 ± 0.06	1.15 ± 0.07	1.18 ± 0.07	1.38 ± 0.08	1.56 ± 0.09
3065 ± 3	0.97 ± 0.06	1.02 ± 0.06	1.03 ± 0.06	1.13 ± 0.07	1.24 ± 0.07	1.35 ± 0.08
3115 ± 3	1.02 ± 0.06	0.94 ± 0.06	1.08 ± 0.06	1.07 ± 0.06	1.17 ± 0.07	1.28 ± 0.07
3165 ± 3	0.97 ± 0.06	0.96 ± 0.06	1.01 ± 0.06	1.08 ± 0.06	1.23 ± 0.07	1.27 ± 0.07
3215 ± 3	1.01 ± 0.06	1.05 ± 0.06	1.04 ± 0.06	1.08 ± 0.06	1.19 ± 0.07	1.23 ± 0.07
3265 ± 3	1.00 ± 0.06	0.96 ± 0.06	0.97 ± 0.06	1.10 ± 0.07	1.11 ± 0.06	1.12 ± 0.07
3314 ± 3	0.91 ± 0.05	0.89 ± 0.05	0.98 ± 0.06	0.95 ± 0.06	1.08 ± 0.06	1.11 ± 0.06
3364 ± 3	0.92 ± 0.06	0.88 ± 0.05	1.02 ± 0.06	0.98 ± 0.06	1.07 ± 0.06	1.15 ± 0.07
3414 ± 3	0.93 ± 0.06	0.92 ± 0.06	0.93 ± 0.05	0.99 ± 0.06	1.07 ± 0.06	1.03 ± 0.06
3464 ± 3	0.88 ± 0.05	0.93 ± 0.05	0.93 ± 0.05	0.90 ± 0.05	1.01 ± 0.06	1.10 ± 0.06
3514 ± 3	0.85 ± 0.05	0.89 ± 0.05	0.93 ± 0.05	0.97 ± 0.05	0.95 ± 0.05	0.97 ± 0.06
3564 ± 3	0.88 ± 0.05	0.87 ± 0.05	0.89 ± 0.05	0.97 ± 0.06	0.95 ± 0.06	1.00 ± 0.06
3614 ± 3	0.80 ± 0.05	0.86 ± 0.05	0.88 ± 0.05	0.92 ± 0.05	0.92 ± 0.05	0.93 ± 0.06
3664 ± 3	0.78 ± 0.05	0.81 ± 0.05	0.89 ± 0.05	0.89 ± 0.05	0.92 ± 0.05	0.99 ± 0.06
3713 ± 3	0.79 ± 0.05	0.79 ± 0.05	0.85 ± 0.05	0.86 ± 0.05	0.88 ± 0.05	0.86 ± 0.05
3763 ± 3	0.75 ± 0.04	0.82 ± 0.05	0.82 ± 0.05	0.87 ± 0.05	0.88 ± 0.05	0.83 ± 0.05
3813 ± 3	0.79 ± 0.05	0.82 ± 0.05	0.81 ± 0.05	0.83 ± 0.05	0.82 ± 0.05	0.84 ± 0.05
3863 ± 3	0.72 ± 0.04	0.77 ± 0.05	0.83 ± 0.05	0.79 ± 0.05	0.80 ± 0.05	0.82 ± 0.05
3913 ± 3	0.76 ± 0.04	0.77 ± 0.04	0.73 ± 0.04	0.80 ± 0.05	0.81 ± 0.05	0.77 ± 0.04
3963 ± 3	0.73 ± 0.04	0.76 ± 0.04	0.71 ± 0.04	0.76 ± 0.04	0.76 ± 0.04	0.79 ± 0.05
4013 ± 3	0.72 ± 0.04	0.74 ± 0.04	0.77 ± 0.04	0.72 ± 0.04	0.82 ± 0.05	0.82 ± 0.05
4063 ± 3	0.74 ± 0.04	0.73 ± 0.04	0.72 ± 0.04	0.68 ± 0.04	0.78 ± 0.04	0.80 ± 0.04
4112 ± 3	0.72 ± 0.04	0.72 ± 0.04	0.70 ± 0.04	0.73 ± 0.04	0.80 ± 0.04	0.84 ± 0.05
4162 ± 3	0.67 ± 0.04	0.65 ± 0.04	0.67 ± 0.04	0.71 ± 0.04	0.77 ± 0.04	0.80 ± 0.04
4212 ± 3	0.69 ± 0.04	0.66 ± 0.04	0.67 ± 0.04	0.72 ± 0.04	0.75 ± 0.04	0.80 ± 0.04
4262 ± 3	0.72 ± 0.04	0.68 ± 0.04	0.69 ± 0.04	0.70 ± 0.04	0.77 ± 0.04	0.79 ± 0.04
4312 ± 3	0.69 ± 0.04	0.66 ± 0.04	0.66 ± 0.04	0.69 ± 0.04	0.74 ± 0.04	0.77 ± 0.04
4362 ± 3	0.71 ± 0.04	0.71 ± 0.04	0.69 ± 0.04	0.69 ± 0.04	0.75 ± 0.04	0.72 ± 0.04

E_{lab} (keV)	dσ/dΩ (mb/sr)					
	120°	130°	140°	150°	160°	170°
4411 ± 3	0.68 ± 0.04	0.70 ± 0.04	0.70 ± 0.04	0.68 ± 0.04	0.75 ± 0.04	0.78 ± 0.04
4461 ± 3	0.68 ± 0.04	0.70 ± 0.04	0.69 ± 0.04	0.74 ± 0.04	0.71 ± 0.04	0.79 ± 0.04
4511 ± 3	0.75 ± 0.04	0.72 ± 0.04	0.66 ± 0.04	0.67 ± 0.04	0.76 ± 0.04	0.83 ± 0.05
4547 ± 3	0.77 ± 0.04	0.68 ± 0.04	0.65 ± 0.04	0.70 ± 0.04	0.73 ± 0.04	0.80 ± 0.04
4597 ± 3	0.75 ± 0.04	0.71 ± 0.04	0.66 ± 0.04	0.72 ± 0.04	0.72 ± 0.04	0.78 ± 0.04
4661 ± 3	0.73 ± 0.04	0.66 ± 0.04	0.68 ± 0.04	0.69 ± 0.04	0.74 ± 0.04	0.77 ± 0.04
4710 ± 3	0.78 ± 0.04	0.70 ± 0.04	0.65 ± 0.04	0.66 ± 0.04	0.74 ± 0.04	0.75 ± 0.04
4760 ± 3	0.81 ± 0.05	0.73 ± 0.04	0.64 ± 0.04	0.64 ± 0.04	0.71 ± 0.04	0.77 ± 0.04
4810 ± 3	0.75 ± 0.04	0.73 ± 0.04	0.71 ± 0.04	0.61 ± 0.04	0.71 ± 0.04	0.80 ± 0.05
4860 ± 3	0.79 ± 0.04	0.77 ± 0.04	0.67 ± 0.04	0.66 ± 0.04	0.69 ± 0.04	-
4910 ± 3	0.81 ± 0.05	0.73 ± 0.04	0.70 ± 0.04	0.67 ± 0.04	0.73 ± 0.04	0.76 ± 0.04
4960 ± 3	0.77 ± 0.04	0.71 ± 0.04	0.65 ± 0.04	0.65 ± 0.04	0.71 ± 0.04	0.69 ± 0.04
5059 ± 3	0.79 ± 0.04	0.76 ± 0.04	0.63 ± 0.04	0.66 ± 0.04	-	0.66 ± 0.04
5159 ± 3	0.78 ± 0.05	0.72 ± 0.04	0.65 ± 0.04	0.62 ± 0.04	-	0.65 ± 0.04
5258 ± 3	0.75 ± 0.04	0.69 ± 0.04	0.63 ± 0.04	-	0.60 ± 0.04	0.62 ± 0.04
5358 ± 3	0.71 ± 0.04	0.69 ± 0.04	0.60 ± 0.04	-	0.55 ± 0.03	0.63 ± 0.04
5458 ± 3	0.73 ± 0.04	0.65 ± 0.04	0.63 ± 0.04	-	0.57 ± 0.03	0.61 ± 0.03
5557 ± 3	0.73 ± 0.04	0.62 ± 0.03	0.60 ± 0.03	-	0.57 ± 0.03	0.63 ± 0.03
5657 ± 3	0.68 ± 0.04	0.60 ± 0.03	0.57 ± 0.03	0.504 ± 0.029	0.58 ± 0.03	0.64 ± 0.04
5756 ± 3	0.71 ± 0.04	0.60 ± 0.03	0.60 ± 0.03	0.501 ± 0.028	0.57 ± 0.03	0.64 ± 0.03
5856 ± 3	0.70 ± 0.04	0.56 ± 0.03	0.60 ± 0.03	0.518 ± 0.029	0.57 ± 0.03	0.60 ± 0.03
5956 ± 3	0.69 ± 0.04	0.60 ± 0.03	-	0.55 ± 0.03	0.58 ± 0.03	0.65 ± 0.04

Table 3

E_{lab} (keV)	dσ/dΩ (mb/sr)					
	120°	130°	140°	150°	160°	170°
1565 ± 3	0.273 ± 0.022	0.295 ± 0.025	0.311 ± 0.024	0.297 ± 0.024	0.284 ± 0.022	0.277 ± 0.023
1665 ± 3	0.334 ± 0.025	0.355 ± 0.026	0.358 ± 0.025	0.43 ± 0.03	0.45 ± 0.03	0.375 ± 0.026
1766 ± 3	0.435 ± 0.029	0.47 ± 0.03	0.51 ± 0.03	0.58 ± 0.04	0.54 ± 0.03	0.55 ± 0.03
1866 ± 3	0.45 ± 0.03	0.55 ± 0.04	0.54 ± 0.04	0.72 ± 0.05	0.63 ± 0.04	0.69 ± 0.04
1916 ± 3	0.50 ± 0.04	0.58 ± 0.05	0.57 ± 0.04	0.69 ± 0.05	0.68 ± 0.05	0.69 ± 0.05
1966 ± 3	0.49 ± 0.03	0.58 ± 0.04	0.62 ± 0.04	0.71 ± 0.04	0.80 ± 0.05	0.79 ± 0.05
2016 ± 3	0.52 ± 0.04	0.57 ± 0.05	0.66 ± 0.05	0.68 ± 0.05	0.79 ± 0.05	0.79 ± 0.06
2066 ± 3	0.49 ± 0.04	0.70 ± 0.05	0.65 ± 0.04	0.79 ± 0.05	0.88 ± 0.05	0.85 ± 0.05
2116 ± 3	0.53 ± 0.04	0.64 ± 0.05	0.61 ± 0.04	0.76 ± 0.06	0.75 ± 0.05	0.86 ± 0.06
2166 ± 3	0.45 ± 0.03	0.61 ± 0.04	0.67 ± 0.04	0.83 ± 0.05	0.78 ± 0.05	0.84 ± 0.05
2266 ± 3	0.52 ± 0.04	0.59 ± 0.04	0.70 ± 0.04	0.75 ± 0.05	0.86 ± 0.05	0.81 ± 0.05
2366 ± 3	0.44 ± 0.03	0.59 ± 0.04	0.68 ± 0.04	0.76 ± 0.05	0.75 ± 0.05	0.81 ± 0.05
2416 ± 3	0.46 ± 0.04	0.59 ± 0.05	0.64 ± 0.05	0.73 ± 0.06	0.67 ± 0.05	0.83 ± 0.06
2466 ± 3	0.42 ± 0.03	0.59 ± 0.04	0.60 ± 0.04	0.68 ± 0.04	0.71 ± 0.05	0.78 ± 0.05
2516 ± 3	0.48 ± 0.05	0.51 ± 0.05	0.63 ± 0.06	0.69 ± 0.06	0.66 ± 0.06	0.75 ± 0.06
2566 ± 3	0.44 ± 0.04	0.57 ± 0.04	0.62 ± 0.04	0.60 ± 0.04	0.62 ± 0.04	0.72 ± 0.05
2666 ± 3	0.43 ± 0.04	0.50 ± 0.04	0.56 ± 0.04	0.60 ± 0.04	0.63 ± 0.04	0.69 ± 0.05
2765 ± 3	0.40 ± 0.04	0.46 ± 0.04	0.54 ± 0.04	0.55 ± 0.04	0.55 ± 0.04	0.61 ± 0.04
2865 ± 3	0.38 ± 0.03	0.44 ± 0.04	0.45 ± 0.04	0.53 ± 0.04	0.47 ± 0.03	0.47 ± 0.04
2956 ± 3	0.34 ± 0.03	0.41 ± 0.04	0.50 ± 0.04	0.49 ± 0.04	0.46 ± 0.03	0.45 ± 0.03
3065 ± 3	0.40 ± 0.03	0.41 ± 0.03	0.43 ± 0.03	0.48 ± 0.04	0.46 ± 0.03	0.42 ± 0.03
3115 ± 3	0.37 ± 0.04	0.44 ± 0.04	0.48 ± 0.03	0.50 ± 0.04	0.42 ± 0.03	0.43 ± 0.03
3165 ± 3	0.40 ± 0.03	0.41 ± 0.03	0.49 ± 0.03	0.49 ± 0.03	0.50 ± 0.03	0.42 ± 0.03
3215 ± 3	0.46 ± 0.04	0.51 ± 0.04	0.51 ± 0.04	0.48 ± 0.04	0.48 ± 0.03	0.50 ± 0.04
3265 ± 3	0.39 ± 0.03	0.51 ± 0.04	0.51 ± 0.04	0.52 ± 0.04	0.53 ± 0.04	0.49 ± 0.04
3314 ± 3	0.45 ± 0.03	0.45 ± 0.03	0.57 ± 0.04	0.56 ± 0.04	0.51 ± 0.04	0.48 ± 0.03
3364 ± 3	0.42 ± 0.03	0.47 ± 0.04	0.57 ± 0.04	0.54 ± 0.04	0.51 ± 0.04	0.52 ± 0.04
3414 ± 3	0.41 ± 0.03	0.53 ± 0.04	0.54 ± 0.04	0.58 ± 0.04	0.55 ± 0.04	0.60 ± 0.04
3464 ± 3	0.41 ± 0.03	0.49 ± 0.03	0.58 ± 0.04	0.54 ± 0.04	0.55 ± 0.03	0.52 ± 0.03
3514 ± 3	0.331 ± 0.026	0.49 ± 0.03	0.57 ± 0.04	0.60 ± 0.04	0.55 ± 0.03	0.58 ± 0.04
3564 ± 3	0.45 ± 0.03	0.51 ± 0.04	0.61 ± 0.04	0.61 ± 0.04	0.59 ± 0.04	0.57 ± 0.04
3614 ± 3	0.42 ± 0.03	0.51 ± 0.04	0.54 ± 0.04	0.60 ± 0.04	0.56 ± 0.04	0.59 ± 0.04
3664 ± 3	0.39 ± 0.03	0.52 ± 0.04	0.58 ± 0.04	0.60 ± 0.04	0.63 ± 0.04	0.57 ± 0.04
3713 ± 3	0.401 ± 0.029	0.58 ± 0.04	0.58 ± 0.04	0.67 ± 0.04	0.61 ± 0.04	0.57 ± 0.04
3763 ± 3	0.42 ± 0.03	0.52 ± 0.04	0.61 ± 0.04	0.63 ± 0.04	0.63 ± 0.04	0.58 ± 0.04
3813 ± 3	0.411 ± 0.029	0.55 ± 0.04	0.58 ± 0.04	0.70 ± 0.04	0.64 ± 0.04	0.56 ± 0.04
3863 ± 3	0.43 ± 0.03	0.51 ± 0.04	0.64 ± 0.04	0.68 ± 0.04	0.58 ± 0.04	0.57 ± 0.04
3913 ± 3	0.45 ± 0.03	0.52 ± 0.04	0.56 ± 0.04	0.64 ± 0.04	0.56 ± 0.03	0.58 ± 0.04
3963 ± 3	0.44 ± 0.03	0.55 ± 0.04	0.59 ± 0.04	0.61 ± 0.04	0.57 ± 0.03	0.59 ± 0.04
4013 ± 3	0.43 ± 0.03	0.61 ± 0.04	0.58 ± 0.04	0.61 ± 0.04	0.58 ± 0.04	0.58 ± 0.04
4063 ± 3	0.444 ± 0.029	0.57 ± 0.04	0.61 ± 0.04	0.64 ± 0.04	0.58 ± 0.03	0.55 ± 0.03
4112 ± 3	0.47 ± 0.03	0.58 ± 0.04	0.58 ± 0.03	0.58 ± 0.03	0.59 ± 0.03	0.55 ± 0.03
4162 ± 3	0.48 ± 0.03	0.55 ± 0.04	0.60 ± 0.04	0.62 ± 0.04	0.59 ± 0.04	0.53 ± 0.03
4212 ± 3	0.448 ± 0.029	0.57 ± 0.04	0.59 ± 0.04	0.58 ± 0.04	0.54 ± 0.03	0.52 ± 0.03
4262 ± 3	0.47 ± 0.03	0.57 ± 0.04	0.57 ± 0.03	0.60 ± 0.04	0.55 ± 0.03	0.49 ± 0.03
4312 ± 3	0.48 ± 0.03	0.58 ± 0.04	0.55 ± 0.03	0.61 ± 0.04	0.54 ± 0.03	0.47 ± 0.03
4362 ± 3	0.443 ± 0.027	0.56 ± 0.03	0.55 ± 0.03	0.59 ± 0.04	0.54 ± 0.03	0.49 ± 0.03

E_{lab} (keV)	dσ/dΩ (mb/sr)					
	120°	130°	140°	150°	160°	170°
4411 ± 3	0.48 ± 0.03	0.58 ± 0.04	0.54 ± 0.03	0.55 ± 0.03	0.52 ± 0.03	0.455 ± 0.029
4461 ± 3	0.51 ± 0.03	0.59 ± 0.04	0.53 ± 0.03	0.55 ± 0.04	0.52 ± 0.03	0.428 ± 0.029
4511 ± 3	0.48 ± 0.03	0.56 ± 0.04	0.55 ± 0.03	0.52 ± 0.04	0.50 ± 0.03	0.440 ± 0.029
4547 ± 3	0.51 ± 0.03	0.52 ± 0.03	0.55 ± 0.03	0.55 ± 0.03	0.51 ± 0.03	0.456 ± 0.028
4597 ± 3	0.49 ± 0.03	0.59 ± 0.04	0.55 ± 0.03	0.52 ± 0.04	0.44 ± 0.03	0.46 ± 0.03
4661 ± 3	0.47 ± 0.03	0.56 ± 0.04	0.56 ± 0.04	0.50 ± 0.03	0.425 ± 0.028	0.44 ± 0.03
4710 ± 3	0.49 ± 0.03	0.52 ± 0.03	0.54 ± 0.03	0.52 ± 0.03	0.465 ± 0.029	0.432 ± 0.028
4760 ± 3	0.52 ± 0.03	0.51 ± 0.03	0.58 ± 0.04	0.47 ± 0.04	0.445 ± 0.029	0.401 ± 0.028
4810 ± 3	0.48 ± 0.03	0.54 ± 0.04	0.53 ± 0.03	0.47 ± 0.03	0.420 ± 0.028	0.370 ± 0.027
4860 ± 3	0.46 ± 0.03	0.51 ± 0.03	0.56 ± 0.03	0.48 ± 0.03	0.435 ± 0.029	0.421 ± 0.029
4910 ± 3	0.50 ± 0.03	0.52 ± 0.03	0.53 ± 0.03	0.47 ± 0.03	0.431 ± 0.029	0.359 ± 0.026
4960 ± 3	0.46 ± 0.03	0.53 ± 0.03	0.51 ± 0.03	0.48 ± 0.03	0.423 ± 0.029	0.371 ± 0.026
5059 ± 3	0.52 ± 0.03	0.53 ± 0.03	0.53 ± 0.03	0.49 ± 0.03	0.398 ± 0.027	0.348 ± 0.026
5159 ± 3	0.50 ± 0.03	0.50 ± 0.03	0.53 ± 0.03	0.48 ± 0.04	0.391 ± 0.029	0.359 ± 0.028
5258 ± 3	0.47 ± 0.03	0.54 ± 0.04	0.53 ± 0.03	0.45 ± 0.03	0.366 ± 0.026	0.335 ± 0.027
5358 ± 3	0.47 ± 0.03	0.55 ± 0.04	0.51 ± 0.03	0.51 ± 0.03	0.371 ± 0.026	0.301 ± 0.024
5458 ± 3	0.49 ± 0.03	0.49 ± 0.03	0.50 ± 0.03	0.46 ± 0.03	0.355 ± 0.025	0.280 ± 0.022
5557 ± 3	0.476 ± 0.028	0.50 ± 0.03	0.497 ± 0.029	0.448 ± 0.029	0.366 ± 0.024	0.326 ± 0.024
5657 ± 3	0.50 ± 0.03	0.458 ± 0.029	0.52 ± 0.03	0.45 ± 0.03	0.385 ± 0.026	0.318 ± 0.023
5756 ± 3	0.438 ± 0.027	0.475 ± 0.029	0.475 ± 0.028	0.466 ± 0.029	0.368 ± 0.025	0.288 ± 0.021
5856 ± 3	0.429 ± 0.026	0.445 ± 0.027	0.434 ± 0.027	0.421 ± 0.027	0.338 ± 0.022	0.311 ± 0.023
5956 ± 3	0.420 ± 0.027	0.443 ± 0.028	0.422 ± 0.028	0.48 ± 0.03	0.371 ± 0.026	0.296 ± 0.022

Table 4

E_{lab} (keV)	dσ/dΩ (mb/sr)					
	120°	130°	140°	150°	160°	170°
1565 ± 3	0.375 ± 0.028	0.342 ± 0.027	0.388 ± 0.027	0.324 ± 0.025	0.298 ± 0.024	0.298 ± 0.023
1665 ± 3	0.442 ± 0.029	0.48 ± 0.03	0.416 ± 0.028	0.46 ± 0.03	0.426 ± 0.029	0.398 ± 0.028
1766 ± 3	0.58 ± 0.04	0.59 ± 0.04	0.55 ± 0.03	0.53 ± 0.03	0.49 ± 0.03	0.45 ± 0.03
1866 ± 3	0.59 ± 0.04	0.61 ± 0.04	0.53 ± 0.03	0.51 ± 0.03	0.46 ± 0.03	0.414 ± 0.029
1916 ± 3	0.66 ± 0.05	0.64 ± 0.05	0.56 ± 0.04	0.54 ± 0.04	0.44 ± 0.04	0.45 ± 0.04
1966 ± 3	0.62 ± 0.04	0.60 ± 0.04	0.60 ± 0.04	0.50 ± 0.03	0.45 ± 0.03	0.399 ± 0.028
2016 ± 3	0.63 ± 0.05	0.62 ± 0.05	0.49 ± 0.04	0.51 ± 0.04	0.38 ± 0.03	0.35 ± 0.03
2066 ± 3	0.64 ± 0.04	0.62 ± 0.04	0.54 ± 0.04	0.46 ± 0.03	0.41 ± 0.03	0.355 ± 0.027
2116 ± 3	0.57 ± 0.04	0.62 ± 0.05	0.53 ± 0.04	0.47 ± 0.04	0.312 ± 0.029	0.296 ± 0.028
2166 ± 3	0.50 ± 0.04	0.52 ± 0.04	0.46 ± 0.03	0.359 ± 0.029	0.343 ± 0.027	0.250 ± 0.022
2266 ± 3	0.54 ± 0.04	0.54 ± 0.04	0.49 ± 0.03	0.367 ± 0.029	0.335 ± 0.026	0.262 ± 0.023
2366 ± 3	0.51 ± 0.04	0.52 ± 0.04	0.52 ± 0.04	0.380 ± 0.029	0.286 ± 0.024	0.215 ± 0.021
2416 ± 3	0.65 ± 0.05	0.56 ± 0.05	0.49 ± 0.04	0.32 ± 0.03	0.30 ± 0.03	0.262 ± 0.029
2466 ± 3	0.52 ± 0.04	0.56 ± 0.04	0.48 ± 0.03	0.374 ± 0.029	0.340 ± 0.026	0.284 ± 0.024
2516 ± 3	0.52 ± 0.05	0.65 ± 0.06	0.47 ± 0.04	0.44 ± 0.04	0.34 ± 0.04	0.28 ± 0.03
2566 ± 3	0.53 ± 0.04	0.58 ± 0.04	0.44 ± 0.03	0.45 ± 0.04	0.40 ± 0.03	0.359 ± 0.029
2666 ± 3	0.58 ± 0.04	0.57 ± 0.04	0.48 ± 0.04	0.44 ± 0.03	0.39 ± 0.03	0.35 ± 0.03
2765 ± 3	0.53 ± 0.04	0.56 ± 0.04	0.53 ± 0.04	0.48 ± 0.04	0.45 ± 0.03	0.37 ± 0.03
2865 ± 3	0.60 ± 0.04	0.54 ± 0.04	0.50 ± 0.04	0.46 ± 0.03	0.47 ± 0.03	0.47 ± 0.03
2956 ± 3	0.59 ± 0.04	0.55 ± 0.04	0.61 ± 0.04	0.53 ± 0.04	0.49 ± 0.03	0.57 ± 0.04
3065 ± 3	0.65 ± 0.04	0.58 ± 0.04	0.56 ± 0.04	0.59 ± 0.04	0.62 ± 0.04	0.60 ± 0.04
3115 ± 3	0.63 ± 0.04	0.65 ± 0.04	0.61 ± 0.04	0.56 ± 0.04	0.67 ± 0.04	0.65 ± 0.04
3165 ± 3	0.68 ± 0.04	0.66 ± 0.04	0.58 ± 0.04	0.66 ± 0.04	0.70 ± 0.04	0.68 ± 0.04
3215 ± 3	0.77 ± 0.05	0.65 ± 0.04	0.64 ± 0.04	0.63 ± 0.04	0.73 ± 0.05	0.70 ± 0.05
3265 ± 3	0.59 ± 0.04	0.70 ± 0.05	0.67 ± 0.04	0.67 ± 0.04	0.75 ± 0.05	0.75 ± 0.05
3314 ± 3	0.66 ± 0.04	0.68 ± 0.04	0.65 ± 0.04	0.71 ± 0.04	0.74 ± 0.05	0.77 ± 0.05
3364 ± 3	0.62 ± 0.04	0.64 ± 0.04	0.66 ± 0.04	0.68 ± 0.04	0.73 ± 0.04	0.77 ± 0.05
3414 ± 3	0.62 ± 0.04	0.70 ± 0.05	0.63 ± 0.04	0.73 ± 0.05	0.75 ± 0.05	0.91 ± 0.05
3464 ± 3	0.62 ± 0.04	0.62 ± 0.04	0.60 ± 0.04	0.67 ± 0.04	0.80 ± 0.05	0.81 ± 0.05
3514 ± 3	0.60 ± 0.04	0.59 ± 0.04	0.67 ± 0.04	0.70 ± 0.04	0.74 ± 0.04	0.87 ± 0.05
3564 ± 3	0.56 ± 0.04	0.58 ± 0.04	0.61 ± 0.04	0.75 ± 0.05	0.84 ± 0.05	0.88 ± 0.05
3614 ± 3	0.58 ± 0.04	0.57 ± 0.04	0.65 ± 0.04	0.64 ± 0.04	0.78 ± 0.05	0.86 ± 0.05
3664 ± 3	0.55 ± 0.04	0.57 ± 0.04	0.61 ± 0.04	0.64 ± 0.04	0.77 ± 0.05	0.87 ± 0.05
3713 ± 3	0.55 ± 0.04	0.58 ± 0.04	0.61 ± 0.04	0.76 ± 0.05	0.78 ± 0.05	0.89 ± 0.05
3763 ± 3	0.50 ± 0.03	0.54 ± 0.03	0.61 ± 0.04	0.73 ± 0.04	0.86 ± 0.05	0.87 ± 0.05
3813 ± 3	0.49 ± 0.03	0.56 ± 0.03	0.56 ± 0.03	0.76 ± 0.04	0.84 ± 0.05	0.89 ± 0.05
3863 ± 3	0.49 ± 0.03	0.58 ± 0.04	0.64 ± 0.04	0.69 ± 0.04	0.88 ± 0.05	0.93 ± 0.05
3913 ± 3	0.53 ± 0.03	0.52 ± 0.03	0.66 ± 0.04	0.78 ± 0.04	0.83 ± 0.05	0.91 ± 0.05
3963 ± 3	0.55 ± 0.03	0.56 ± 0.04	0.62 ± 0.04	0.71 ± 0.04	0.86 ± 0.05	0.92 ± 0.05
4013 ± 3	0.52 ± 0.03	0.59 ± 0.04	0.68 ± 0.04	0.73 ± 0.04	0.84 ± 0.05	0.97 ± 0.05
4063 ± 3	0.46 ± 0.03	0.56 ± 0.03	0.61 ± 0.04	0.78 ± 0.04	0.85 ± 0.05	0.99 ± 0.05
4112 ± 3	0.54 ± 0.03	0.53 ± 0.03	0.62 ± 0.04	0.71 ± 0.04	0.81 ± 0.04	0.98 ± 0.05
4162 ± 3	0.51 ± 0.03	0.56 ± 0.04	0.59 ± 0.04	0.71 ± 0.04	0.82 ± 0.05	0.94 ± 0.05
4212 ± 3	0.52 ± 0.03	0.56 ± 0.03	0.58 ± 0.03	0.76 ± 0.04	0.84 ± 0.05	0.88 ± 0.05
4262 ± 3	0.52 ± 0.03	0.56 ± 0.03	0.63 ± 0.04	0.70 ± 0.04	0.87 ± 0.05	0.88 ± 0.05
4312 ± 3	0.48 ± 0.03	0.53 ± 0.03	0.56 ± 0.03	0.71 ± 0.04	0.82 ± 0.05	0.87 ± 0.05
4362 ± 3	0.53 ± 0.03	0.54 ± 0.03	0.63 ± 0.03	0.67 ± 0.04	0.78 ± 0.04	0.91 ± 0.05

E_{lab} (keV)	dσ/dΩ (mb/sr)					
	120°	130°	140°	150°	160°	170°
4411 ± 3	0.51 ± 0.03	0.56 ± 0.03	0.58 ± 0.03	0.67 ± 0.04	0.79 ± 0.04	0.91 ± 0.05
4461 ± 3	0.51 ± 0.03	0.53 ± 0.03	0.61 ± 0.04	0.67 ± 0.04	0.82 ± 0.05	0.90 ± 0.05
4511 ± 3	0.48 ± 0.03	0.59 ± 0.03	0.62 ± 0.04	0.69 ± 0.04	0.81 ± 0.04	0.86 ± 0.05
4547 ± 3	0.441 ± 0.026	0.51 ± 0.03	0.60 ± 0.03	0.71 ± 0.04	0.76 ± 0.04	0.86 ± 0.05
4597 ± 3	0.48 ± 0.03	0.53 ± 0.03	0.59 ± 0.03	0.70 ± 0.04	0.76 ± 0.04	0.85 ± 0.05
4661 ± 3	0.50 ± 0.03	0.53 ± 0.03	0.58 ± 0.03	0.68 ± 0.04	0.81 ± 0.05	0.86 ± 0.05
4710 ± 3	0.46 ± 0.03	0.56 ± 0.03	0.58 ± 0.03	0.69 ± 0.04	0.81 ± 0.04	0.84 ± 0.05
4760 ± 3	0.47 ± 0.03	0.52 ± 0.03	0.58 ± 0.03	0.67 ± 0.04	0.75 ± 0.04	0.84 ± 0.05
4810 ± 3	0.46 ± 0.03	0.49 ± 0.03	0.58 ± 0.04	0.61 ± 0.04	0.74 ± 0.04	0.85 ± 0.05
4860 ± 3	0.428 ± 0.028	0.56 ± 0.03	0.58 ± 0.03	0.70 ± 0.04	0.79 ± 0.04	0.79 ± 0.04
4910 ± 3	0.463 ± 0.029	0.51 ± 0.03	0.59 ± 0.03	0.69 ± 0.04	0.76 ± 0.04	0.84 ± 0.05
4960 ± 3	0.372 ± 0.025	0.53 ± 0.03	0.55 ± 0.03	0.69 ± 0.04	0.78 ± 0.04	0.81 ± 0.05
5059 ± 3	0.442 ± 0.029	0.54 ± 0.03	0.58 ± 0.03	0.64 ± 0.04	0.75 ± 0.04	0.84 ± 0.05
5159 ± 3	0.44 ± 0.03	0.50 ± 0.03	0.53 ± 0.03	0.64 ± 0.04	0.75 ± 0.04	0.75 ± 0.04
5258 ± 3	0.404 ± 0.028	0.45 ± 0.03	0.49 ± 0.03	0.61 ± 0.04	0.69 ± 0.04	0.74 ± 0.04
5358 ± 3	0.405 ± 0.028	0.48 ± 0.03	0.52 ± 0.03	0.56 ± 0.03	0.70 ± 0.04	0.71 ± 0.04
5458 ± 3	0.371 ± 0.025	0.415 ± 0.027	0.474 ± 0.029	0.58 ± 0.03	0.65 ± 0.04	0.71 ± 0.04
5557 ± 3	0.403 ± 0.025	0.436 ± 0.026	0.464 ± 0.027	0.55 ± 0.03	0.61 ± 0.03	0.65 ± 0.04
5657 ± 3	0.360 ± 0.024	0.402 ± 0.026	0.408 ± 0.025	0.51 ± 0.03	0.60 ± 0.03	0.64 ± 0.04
5756 ± 3	0.392 ± 0.024	0.378 ± 0.024	0.450 ± 0.026	0.468 ± 0.027	0.55 ± 0.03	0.59 ± 0.03
5856 ± 3	0.371 ± 0.023	0.400 ± 0.025	0.408 ± 0.024	0.456 ± 0.027	0.493 ± 0.028	0.56 ± 0.03
5956 ± 3	0.373 ± 0.025	0.334 ± 0.023	0.360 ± 0.023	0.441 ± 0.027	0.460 ± 0.027	0.505 ± 0.029

Table 5

E_{lab} (keV)	dσ/dΩ (mb/sr)					
	120°	130°	140°	150°	160°	170°
1565 ± 3	-	0.134 ± 0.016	0.129 ± 0.015	0.153 ± 0.016	0.134 ± 0.015	0.148 ± 0.016
1665 ± 3	0.173 ± 0.016	0.186 ± 0.018	0.190 ± 0.016	0.211 ± 0.019	0.200 ± 0.017	0.191 ± 0.016
1766 ± 3	0.208 ± 0.018	0.250 ± 0.021	0.242 ± 0.019	0.294 ± 0.022	0.307 ± 0.022	0.335 ± 0.024
1866 ± 3	0.268 ± 0.023	0.313 ± 0.026	0.305 ± 0.025	0.301 ± 0.024	0.393 ± 0.029	0.362 ± 0.027
1916 ± 3	0.30 ± 0.03	0.36 ± 0.03	0.33 ± 0.03	0.41 ± 0.04	0.41 ± 0.04	0.36 ± 0.03
1966 ± 3	0.328 ± 0.025	0.354 ± 0.026	0.302 ± 0.023	0.365 ± 0.027	0.411 ± 0.029	0.408 ± 0.029
2016 ± 3	0.31 ± 0.03	0.36 ± 0.04	0.38 ± 0.03	0.41 ± 0.04	0.38 ± 0.03	0.37 ± 0.03
2066 ± 3	0.38 ± 0.03	0.372 ± 0.029	0.372 ± 0.028	0.37 ± 0.03	0.40 ± 0.03	0.44 ± 0.03
2116 ± 3	0.34 ± 0.03	0.40 ± 0.04	0.42 ± 0.04	0.40 ± 0.03	0.42 ± 0.04	0.46 ± 0.04
2166 ± 3	0.346 ± 0.028	0.324 ± 0.028	0.374 ± 0.029	0.44 ± 0.03	0.45 ± 0.03	0.52 ± 0.04
2266 ± 3	0.38 ± 0.03	0.40 ± 0.03	0.45 ± 0.03	0.45 ± 0.03	0.52 ± 0.04	0.50 ± 0.03
2366 ± 3	0.38 ± 0.03	0.48 ± 0.04	0.49 ± 0.03	0.53 ± 0.04	0.65 ± 0.04	0.56 ± 0.04
2416 ± 3	0.46 ± 0.04	0.47 ± 0.04	0.55 ± 0.04	0.52 ± 0.04	0.65 ± 0.05	0.64 ± 0.05
2466 ± 3	0.43 ± 0.03	0.54 ± 0.04	0.53 ± 0.04	0.63 ± 0.04	0.66 ± 0.04	0.65 ± 0.04
2516 ± 3	0.52 ± 0.05	0.48 ± 0.05	0.61 ± 0.05	0.67 ± 0.06	0.73 ± 0.06	0.74 ± 0.06
2566 ± 3	0.54 ± 0.04	0.57 ± 0.04	-	0.76 ± 0.05	0.80 ± 0.05	0.80 ± 0.05
2666 ± 3	0.54 ± 0.04	0.58 ± 0.04	-	-	-	0.85 ± 0.05
2765 ± 3	0.56 ± 0.04	0.59 ± 0.04	-	-	-	-
2865 ± 3	0.62 ± 0.04	-	-	-	-	-
3464 ± 3	-	-	-	-	-	0.70 ± 0.04
3514 ± 3	-	-	-	-	-	0.68 ± 0.04
3564 ± 3	-	-	-	-	0.70 ± 0.04	0.72 ± 0.04
3614 ± 3	-	-	-	-	0.77 ± 0.05	0.68 ± 0.04
3664 ± 3	-	-	-	-	0.74 ± 0.04	0.66 ± 0.04
3713 ± 3	-	-	-	-	0.73 ± 0.04	0.66 ± 0.04
3763 ± 3	-	-	-	-	0.68 ± 0.04	0.62 ± 0.04
3813 ± 3	-	-	-	0.71 ± 0.04	0.66 ± 0.04	0.66 ± 0.04
3863 ± 3	-	-	-	0.73 ± 0.05	0.66 ± 0.04	0.68 ± 0.04
3913 ± 3	-	-	-	0.72 ± 0.04	0.66 ± 0.04	0.61 ± 0.04
3963 ± 3	-	-	-	0.67 ± 0.04	0.67 ± 0.04	0.60 ± 0.04
4013 ± 3	-	-	-	0.68 ± 0.04	0.66 ± 0.04	0.60 ± 0.04
4063 ± 3	-	-	-	0.67 ± 0.04	0.62 ± 0.04	0.62 ± 0.04
4112 ± 3	-	-	-	0.65 ± 0.04	0.64 ± 0.04	0.57 ± 0.03
4162 ± 3	-	-	-	0.64 ± 0.04	0.63 ± 0.04	0.57 ± 0.03
4212 ± 3	-	-	0.66 ± 0.04	0.63 ± 0.04	0.62 ± 0.04	0.54 ± 0.03
4262 ± 3	-	-	0.67 ± 0.04	0.65 ± 0.04	0.59 ± 0.04	0.55 ± 0.03
4312 ± 3	-	-	0.67 ± 0.04	0.65 ± 0.04	0.60 ± 0.03	0.52 ± 0.03
4362 ± 3	-	-	0.69 ± 0.04	0.64 ± 0.04	0.59 ± 0.03	0.54 ± 0.03
4411 ± 3	-	-	0.65 ± 0.04	0.62 ± 0.04	0.60 ± 0.03	0.54 ± 0.03
4461 ± 3	-	-	0.69 ± 0.04	0.66 ± 0.04	0.60 ± 0.04	0.477 ± 0.029
4511 ± 3	-	-	0.73 ± 0.04	0.63 ± 0.04	0.59 ± 0.03	0.50 ± 0.03
4547 ± 3	-	0.64 ± 0.04	0.69 ± 0.04	0.66 ± 0.04	0.61 ± 0.03	0.459 ± 0.027
4597 ± 3	-	0.70 ± 0.04	0.66 ± 0.04	0.64 ± 0.04	0.59 ± 0.04	0.52 ± 0.03
4661 ± 3	-	0.68 ± 0.04	0.68 ± 0.04	0.65 ± 0.04	0.57 ± 0.03	0.49 ± 0.03
4710 ± 3	-	0.68 ± 0.04	0.69 ± 0.04	0.63 ± 0.04	0.59 ± 0.03	0.50 ± 0.03
4760 ± 3	-	0.68 ± 0.04	0.68 ± 0.04	0.67 ± 0.04	0.62 ± 0.04	0.50 ± 0.03
4810 ± 3	-	0.69 ± 0.04	0.64 ± 0.04	0.64 ± 0.04	0.57 ± 0.03	0.51 ± 0.03

E_{lab} (keV)	$d\sigma/d\Omega$ (mb/sr)					
	120°	130°	140°	150°	160°	170°
4860 ± 3	-	0.70 ± 0.04	0.71 ± 0.04	0.68 ± 0.04	0.57 ± 0.03	0.58 ± 0.03
4910 ± 3	-	0.67 ± 0.04	0.69 ± 0.04	0.66 ± 0.04	0.64 ± 0.04	0.61 ± 0.04
4960 ± 3	-	0.68 ± 0.04	0.70 ± 0.04	0.64 ± 0.04	0.61 ± 0.04	0.57 ± 0.03
5059 ± 3	-	0.64 ± 0.04	0.67 ± 0.04	0.69 ± 0.04	0.65 ± 0.04	0.60 ± 0.04
5159 ± 3	-	0.69 ± 0.04	0.67 ± 0.04	0.66 ± 0.04	0.69 ± 0.04	0.65 ± 0.04
5258 ± 3	0.47 ± 0.03	0.64 ± 0.04	0.61 ± 0.04	0.72 ± 0.04	0.63 ± 0.04	0.63 ± 0.04
5358 ± 3	0.432 ± 0.029	0.62 ± 0.04	0.66 ± 0.04	0.67 ± 0.04	0.69 ± 0.04	0.68 ± 0.04
5458 ± 3	0.431 ± 0.027	0.58 ± 0.03	0.63 ± 0.04	0.67 ± 0.04	0.64 ± 0.04	0.69 ± 0.04
5557 ± 3	0.442 ± 0.027	0.51 ± 0.03	0.61 ± 0.03	0.69 ± 0.04	0.68 ± 0.04	0.73 ± 0.04
5657 ± 3	0.395 ± 0.025	0.57 ± 0.03	0.60 ± 0.03	0.58 ± 0.03	0.67 ± 0.04	0.70 ± 0.04
5756 ± 3	0.382 ± 0.024	0.50 ± 0.03	0.55 ± 0.03	0.64 ± 0.04	0.67 ± 0.04	0.70 ± 0.04
5856 ± 3	0.400 ± 0.025	0.493 ± 0.029	0.56 ± 0.03	0.60 ± 0.03	0.64 ± 0.03	0.65 ± 0.04
5956 ± 3	0.371 ± 0.025	0.484 ± 0.029	0.54 ± 0.03	0.60 ± 0.03	0.58 ± 0.03	0.66 ± 0.04

Table 6

E_{lab} (keV)	dσ/dΩ (mb/sr)					
	120°	130°	140°	150°	160°	170°
1565 ± 3	0.335 ± 0.026	0.381 ± 0.028	0.375 ± 0.027	0.394 ± 0.029	0.43 ± 0.03	0.48 ± 0.03
1665 ± 3	0.51 ± 0.03	0.46 ± 0.03	0.49 ± 0.03	0.53 ± 0.03	0.55 ± 0.03	0.57 ± 0.04
1766 ± 3	0.58 ± 0.04	0.68 ± 0.04	0.65 ± 0.04	0.76 ± 0.04	0.75 ± 0.04	0.77 ± 0.04
1866 ± 3	0.72 ± 0.04	0.82 ± 0.05	0.83 ± 0.05	0.89 ± 0.05	0.91 ± 0.05	0.91 ± 0.05
1916 ± 3	0.90 ± 0.06	0.85 ± 0.06	0.85 ± 0.06	0.88 ± 0.06	0.96 ± 0.06	0.93 ± 0.06
1966 ± 3	0.88 ± 0.05	0.87 ± 0.05	0.88 ± 0.05	0.99 ± 0.06	1.06 ± 0.06	0.98 ± 0.06
2016 ± 3	0.89 ± 0.06	0.89 ± 0.06	0.96 ± 0.06	0.96 ± 0.06	1.00 ± 0.07	1.03 ± 0.07
2066 ± 3	1.02 ± 0.06	1.07 ± 0.06	1.01 ± 0.06	1.05 ± 0.06	1.10 ± 0.06	1.11 ± 0.06
2116 ± 3	0.96 ± 0.06	0.97 ± 0.06	0.96 ± 0.06	1.00 ± 0.07	1.06 ± 0.07	1.05 ± 0.07
2166 ± 3	0.89 ± 0.05	0.98 ± 0.06	0.98 ± 0.06	1.06 ± 0.06	1.01 ± 0.06	1.05 ± 0.06
2266 ± 3	0.94 ± 0.06	1.01 ± 0.06	0.97 ± 0.06	1.02 ± 0.06	1.10 ± 0.06	1.02 ± 0.06
2366 ± 3	1.05 ± 0.06	1.08 ± 0.06	0.97 ± 0.06	0.97 ± 0.06	1.05 ± 0.06	0.96 ± 0.06
2416 ± 3	1.16 ± 0.07	1.12 ± 0.07	1.05 ± 0.07	1.00 ± 0.07	1.01 ± 0.07	0.91 ± 0.06
2466 ± 3	1.03 ± 0.06	1.05 ± 0.06	1.03 ± 0.06	0.99 ± 0.06	1.02 ± 0.06	1.13 ± 0.07
2516 ± 3	1.12 ± 0.08	1.03 ± 0.08	1.06 ± 0.08	1.12 ± 0.08	1.16 ± 0.08	1.17 ± 0.08
2566 ± 3	1.09 ± 0.07	1.13 ± 0.07	1.10 ± 0.07	1.06 ± 0.07	1.20 ± 0.07	1.08 ± 0.07
2666 ± 3	1.06 ± 0.07	1.12 ± 0.07	1.14 ± 0.07	1.16 ± 0.07	1.19 ± 0.07	1.18 ± 0.07
2765 ± 3	1.07 ± 0.07	1.08 ± 0.07	1.16 ± 0.07	1.23 ± 0.07	1.30 ± 0.08	1.30 ± 0.08
2865 ± 3	1.11 ± 0.07	1.09 ± 0.07	1.15 ± 0.07	1.12 ± 0.07	1.29 ± 0.07	1.35 ± 0.08
2956 ± 3	1.06 ± 0.06	1.06 ± 0.06	1.16 ± 0.07	1.14 ± 0.07	1.30 ± 0.07	1.30 ± 0.07
3065 ± 3	1.04 ± 0.06	1.03 ± 0.06	1.11 ± 0.06	1.14 ± 0.07	1.17 ± 0.07	1.23 ± 0.07
3115 ± 3	1.00 ± 0.06	1.07 ± 0.06	1.06 ± 0.06	1.04 ± 0.06	1.16 ± 0.07	1.15 ± 0.07
3165 ± 3	1.05 ± 0.06	1.01 ± 0.06	1.03 ± 0.06	1.02 ± 0.06	1.12 ± 0.06	1.12 ± 0.06
3215 ± 3	1.06 ± 0.06	1.03 ± 0.06	1.00 ± 0.06	0.94 ± 0.06	1.04 ± 0.06	1.12 ± 0.07
3265 ± 3	1.03 ± 0.06	0.93 ± 0.06	0.97 ± 0.06	0.96 ± 0.06	0.92 ± 0.06	0.99 ± 0.06
3314 ± 3	1.01 ± 0.06	0.93 ± 0.06	0.95 ± 0.06	0.94 ± 0.06	0.94 ± 0.06	0.89 ± 0.05
3364 ± 3	0.99 ± 0.06	0.96 ± 0.06	0.86 ± 0.05	0.89 ± 0.05	0.90 ± 0.05	0.81 ± 0.05
3414 ± 3	0.89 ± 0.06	0.85 ± 0.05	0.82 ± 0.05	0.79 ± 0.05	0.83 ± 0.05	0.83 ± 0.05
3464 ± 3	0.92 ± 0.05	0.86 ± 0.05	0.81 ± 0.05	0.75 ± 0.05	0.66 ± 0.04	0.73 ± 0.04
3514 ± 3	0.91 ± 0.05	0.77 ± 0.05	0.81 ± 0.05	0.65 ± 0.04	0.67 ± 0.04	0.65 ± 0.04
3564 ± 3	0.91 ± 0.05	0.81 ± 0.05	0.74 ± 0.05	0.62 ± 0.04	0.66 ± 0.04	0.62 ± 0.04
3614 ± 3	0.85 ± 0.05	0.70 ± 0.05	0.69 ± 0.04	0.59 ± 0.04	0.54 ± 0.04	0.58 ± 0.04
3664 ± 3	0.78 ± 0.05	0.69 ± 0.04	0.67 ± 0.04	0.59 ± 0.04	0.54 ± 0.04	0.54 ± 0.04
3713 ± 3	0.77 ± 0.05	0.67 ± 0.04	0.70 ± 0.04	0.57 ± 0.04	0.54 ± 0.04	0.50 ± 0.03
3763 ± 3	0.79 ± 0.05	0.71 ± 0.04	0.66 ± 0.04	0.57 ± 0.04	0.54 ± 0.03	0.47 ± 0.03
3813 ± 3	0.68 ± 0.04	0.67 ± 0.04	0.58 ± 0.04	0.58 ± 0.04	0.55 ± 0.03	0.46 ± 0.03
3863 ± 3	0.73 ± 0.05	0.68 ± 0.04	0.65 ± 0.04	0.53 ± 0.04	0.49 ± 0.03	0.48 ± 0.03
3913 ± 3	0.74 ± 0.04	0.66 ± 0.04	0.57 ± 0.04	0.57 ± 0.04	0.50 ± 0.03	0.51 ± 0.03
3963 ± 3	0.71 ± 0.04	0.65 ± 0.04	0.59 ± 0.04	0.58 ± 0.04	0.51 ± 0.03	0.48 ± 0.03
4013 ± 3	0.71 ± 0.04	0.67 ± 0.04	0.59 ± 0.04	0.56 ± 0.04	0.47 ± 0.03	0.51 ± 0.03
4063 ± 3	0.71 ± 0.04	0.67 ± 0.04	0.65 ± 0.04	0.56 ± 0.03	0.50 ± 0.03	0.53 ± 0.03
4112 ± 3	0.72 ± 0.04	0.66 ± 0.04	0.64 ± 0.04	0.59 ± 0.03	0.54 ± 0.03	0.50 ± 0.03
4162 ± 3	0.75 ± 0.04	0.63 ± 0.04	0.62 ± 0.04	0.57 ± 0.04	0.59 ± 0.04	0.55 ± 0.03
4212 ± 3	0.68 ± 0.04	0.72 ± 0.04	0.62 ± 0.04	0.57 ± 0.03	0.59 ± 0.04	0.52 ± 0.03
4262 ± 3	0.74 ± 0.04	0.70 ± 0.04	0.65 ± 0.04	0.64 ± 0.04	0.56 ± 0.03	0.53 ± 0.03
4312 ± 3	0.71 ± 0.04	0.66 ± 0.04	0.64 ± 0.04	0.60 ± 0.04	0.65 ± 0.04	0.64 ± 0.04
4362 ± 3	0.70 ± 0.04	0.70 ± 0.04	0.64 ± 0.04	0.64 ± 0.04	0.64 ± 0.04	0.66 ± 0.04

E_{lab} (keV)	dσ/dΩ (mb/sr)					
	120°	130°	140°	150°	160°	170°
4411 ± 3	0.75 ± 0.04	0.72 ± 0.04	0.62 ± 0.04	0.66 ± 0.04	0.61 ± 0.04	0.69 ± 0.04
4461 ± 3	0.76 ± 0.04	0.77 ± 0.05	0.65 ± 0.04	0.69 ± 0.04	0.70 ± 0.04	0.68 ± 0.04
4511 ± 3	0.75 ± 0.04	0.65 ± 0.04	0.69 ± 0.04	0.67 ± 0.04	0.73 ± 0.05	0.73 ± 0.05
4547 ± 3	0.69 ± 0.04	0.65 ± 0.04	0.69 ± 0.04	0.72 ± 0.04	0.73 ± 0.04	-
4597 ± 3	0.75 ± 0.04	0.76 ± 0.05	0.68 ± 0.04	0.70 ± 0.04	0.79 ± 0.05	-
4661 ± 3	0.73 ± 0.04	0.75 ± 0.04	0.72 ± 0.04	0.76 ± 0.05	-	-
4710 ± 3	0.67 ± 0.04	0.73 ± 0.04	-	-	-	-
4760 ± 3	0.70 ± 0.04	0.71 ± 0.04	-	-	-	-
4810 ± 3	0.72 ± 0.04	0.71 ± 0.04	-	-	-	-
4860 ± 3	0.71 ± 0.04	0.69 ± 0.04	-	-	-	-
4910 ± 3	0.68 ± 0.04	0.67 ± 0.04	-	-	-	-
4960 ± 3	0.66 ± 0.04	0.72 ± 0.04	-	-	-	-
5059 ± 3	0.69 ± 0.04	0.71 ± 0.04	-	-	-	-
5159 ± 3	0.68 ± 0.04	0.71 ± 0.04	-	-	-	-
5258 ± 3	0.67 ± 0.04	-	-	-	-	-
5358 ± 3	0.65 ± 0.04	-	-	-	-	-
5458 ± 3	0.60 ± 0.04	-	-	-	-	-
5557 ± 3	0.65 ± 0.04	-	-	-	-	-
5657 ± 3	0.68 ± 0.04	-	-	-	-	-

Table 7

E_{lab} (keV)	dσ/dΩ (mb/sr)					
	120°	130°	140°	150°	160°	170°
1565 ± 3	0.50 ± 0.03	0.48 ± 0.03	0.48 ± 0.03	0.47 ± 0.03	0.43 ± 0.03	0.397 ± 0.029
1665 ± 3	0.67 ± 0.04	0.67 ± 0.04	0.58 ± 0.04	0.57 ± 0.04	0.60 ± 0.04	0.57 ± 0.04
1766 ± 3	0.81 ± 0.05	0.74 ± 0.04	0.69 ± 0.04	0.65 ± 0.04	0.63 ± 0.04	0.61 ± 0.04
1866 ± 3	0.86 ± 0.05	0.81 ± 0.05	0.73 ± 0.04	0.71 ± 0.04	0.71 ± 0.04	0.69 ± 0.04
1916 ± 3	0.90 ± 0.06	0.88 ± 0.06	0.76 ± 0.05	0.79 ± 0.06	0.71 ± 0.05	0.71 ± 0.05
1966 ± 3	0.89 ± 0.05	0.85 ± 0.05	0.76 ± 0.04	0.80 ± 0.05	0.74 ± 0.04	0.72 ± 0.04
2016 ± 3	0.93 ± 0.06	0.80 ± 0.06	0.79 ± 0.05	0.80 ± 0.06	0.74 ± 0.06	0.72 ± 0.04
2066 ± 3	0.91 ± 0.06	0.89 ± 0.05	0.83 ± 0.05	0.83 ± 0.05	0.74 ± 0.05	0.68 ± 0.04
2116 ± 3	0.95 ± 0.06	0.86 ± 0.06	0.90 ± 0.06	0.75 ± 0.05	0.77 ± 0.05	0.66 ± 0.05
2166 ± 3	0.95 ± 0.06	0.88 ± 0.05	0.81 ± 0.05	0.76 ± 0.05	0.71 ± 0.05	0.63 ± 0.04
2266 ± 3	0.95 ± 0.06	0.86 ± 0.05	0.81 ± 0.05	0.72 ± 0.05	0.71 ± 0.05	0.69 ± 0.04
2366 ± 3	1.00 ± 0.06	0.92 ± 0.06	0.82 ± 0.05	0.72 ± 0.05	0.71 ± 0.05	0.63 ± 0.04
2416 ± 3	0.97 ± 0.07	0.88 ± 0.06	0.84 ± 0.06	0.67 ± 0.05	0.66 ± 0.05	0.63 ± 0.05
2466 ± 3	0.94 ± 0.06	0.86 ± 0.05	0.76 ± 0.05	0.72 ± 0.05	0.61 ± 0.04	0.64 ± 0.04
2516 ± 3	0.96 ± 0.07	0.97 ± 0.07	0.77 ± 0.06	0.68 ± 0.06	0.73 ± 0.06	0.65 ± 0.05
2566 ± 3	0.98 ± 0.06	0.89 ± 0.06	0.81 ± 0.05	0.72 ± 0.05	0.66 ± 0.05	0.65 ± 0.04
2666 ± 3	0.98 ± 0.06	0.89 ± 0.06	0.82 ± 0.05	0.66 ± 0.05	0.68 ± 0.05	0.63 ± 0.04
2765 ± 3	1.04 ± 0.06	0.80 ± 0.05	0.85 ± 0.06	0.74 ± 0.05	0.67 ± 0.05	0.60 ± 0.04
2865 ± 3	0.99 ± 0.05	0.84 ± 0.06	0.81 ± 0.05	0.64 ± 0.04	0.62 ± 0.04	0.60 ± 0.04
2956 ± 3	0.94 ± 0.06	0.84 ± 0.05	0.83 ± 0.05	0.69 ± 0.04	0.54 ± 0.04	0.61 ± 0.04
3065 ± 3	0.82 ± 0.05	0.78 ± 0.05	0.76 ± 0.05	0.67 ± 0.04	0.62 ± 0.04	0.58 ± 0.04
3115 ± 3	0.90 ± 0.05	0.81 ± 0.05	0.68 ± 0.04	0.58 ± 0.04	0.55 ± 0.04	0.56 ± 0.04
3165 ± 3	0.88 ± 0.05	0.80 ± 0.05	0.74 ± 0.04	0.73 ± 0.04	0.61 ± 0.04	0.53 ± 0.03
3215 ± 3	0.90 ± 0.06	0.77 ± 0.05	0.73 ± 0.05	0.68 ± 0.04	0.58 ± 0.04	0.51 ± 0.04
3265 ± 3	0.88 ± 0.06	0.88 ± 0.06	0.74 ± 0.05	0.63 ± 0.04	0.59 ± 0.04	0.52 ± 0.04
3314 ± 3	0.85 ± 0.05	0.80 ± 0.05	0.70 ± 0.04	0.60 ± 0.04	0.60 ± 0.04	0.53 ± 0.04
3364 ± 3	0.80 ± 0.05	0.78 ± 0.05	0.75 ± 0.05	0.62 ± 0.04	0.59 ± 0.04	0.54 ± 0.04
3414 ± 3	0.80 ± 0.05	0.72 ± 0.05	0.67 ± 0.04	0.58 ± 0.04	0.57 ± 0.04	0.53 ± 0.04
3464 ± 3	0.77 ± 0.05	0.69 ± 0.04	0.68 ± 0.04	0.58 ± 0.04	0.58 ± 0.04	0.52 ± 0.03
3514 ± 3	0.78 ± 0.05	0.72 ± 0.04	0.63 ± 0.04	0.55 ± 0.03	0.57 ± 0.04	-
3564 ± 3	0.72 ± 0.05	0.67 ± 0.04	0.64 ± 0.04	0.57 ± 0.04	0.57 ± 0.04	-
3614 ± 3	0.69 ± 0.04	0.68 ± 0.04	0.65 ± 0.04	0.56 ± 0.04	-	-
3664 ± 3	0.65 ± 0.04	0.69 ± 0.04	0.65 ± 0.04	-	-	-
3713 ± 3	0.70 ± 0.04	0.62 ± 0.04	0.66 ± 0.04	-	-	-
3763 ± 3	0.70 ± 0.04	0.61 ± 0.04	0.60 ± 0.04	-	-	-
3813 ± 3	0.70 ± 0.04	0.65 ± 0.04	0.59 ± 0.04	-	-	-
3863 ± 3	0.71 ± 0.04	0.61 ± 0.04	-	-	-	-
3913 ± 3	0.68 ± 0.04	0.64 ± 0.04	-	-	-	-
3963 ± 3	0.67 ± 0.04	0.64 ± 0.04	-	-	-	-
4013 ± 3	0.70 ± 0.04	0.69 ± 0.04	-	-	-	-
4063 ± 3	0.66 ± 0.04	0.66 ± 0.04	-	-	-	-
4112 ± 3	0.66 ± 0.04	-	-	-	-	-
4162 ± 3	0.72 ± 0.04	-	-	-	-	-
4212 ± 3	0.70 ± 0.04	-	-	-	-	-
4262 ± 3	0.70 ± 0.04	-	-	-	-	-
4312 ± 3	0.64 ± 0.04	-	-	-	-	-
4362 ± 3	0.63 ± 0.04	-	-	-	-	-

E_{lab} (keV)	dσ/dΩ (mb/sr)					
	120°	130°	140°	150°	160°	170°
4411 ± 3	0.66 ± 0.04	-	-	-	-	-
4547 ± 3	-	-	-	-	-	0.394 ± 0.024
4597 ± 3	-	-	-	-	-	0.369 ± 0.025
4661 ± 3	-	-	-	-	-	0.366 ± 0.025
4710 ± 3	-	-	-	-	0.363 ± 0.023	0.368 ± 0.024
4760 ± 3	-	-	-	-	0.351 ± 0.024	0.338 ± 0.024
4810 ± 3	-	-	-	0.347 ± 0.026	0.339 ± 0.024	0.314 ± 0.023
4860 ± 3	-	-	0.452 ± 0.029	0.333 ± 0.029	0.317 ± 0.023	-
4910 ± 3	-	-	0.431 ± 0.028	0.36 ± 0.03	0.304 ± 0.021	-
4960 ± 3	-	-	0.458 ± 0.029	0.307 ± 0.029	0.320 ± 0.023	-
5059 ± 3	-	-	0.404 ± 0.027	0.316 ± 0.029	-	-
5159 ± 3	-	0.45 ± 0.03	0.405 ± 0.029	-	-	-
5258 ± 3	-	0.45 ± 0.03	0.353 ± 0.026	-	-	-
5358 ± 3	-	0.44 ± 0.03	-	-	-	-
5458 ± 3	-	0.435 ± 0.029	-	-	-	-
5657 ± 3	-	0.387 ± 0.025	-	-	-	-

Table 8

E_{lab} (keV)	dσ/dΩ (mb/sr)					
	120°	130°	140°	150°	160°	170°
1565 ± 3	0.265 ± 0.022	0.300 ± 0.024	0.278 ± 0.022	0.309 ± 0.025	0.251 ± 0.021	0.247 ± 0.021
1665 ± 3	0.395 ± 0.027	0.403 ± 0.028	0.394 ± 0.027	0.345 ± 0.025	0.344 ± 0.025	0.317 ± 0.024
1766 ± 3	0.48 ± 0.03	0.53 ± 0.03	0.50 ± 0.03	0.52 ± 0.03	0.46 ± 0.03	0.49 ± 0.03
1866 ± 3	0.61 ± 0.04	0.62 ± 0.04	0.61 ± 0.04	0.58 ± 0.04	0.58 ± 0.04	0.58 ± 0.04
1916 ± 3	0.60 ± 0.05	0.66 ± 0.05	0.60 ± 0.04	0.71 ± 0.05	0.64 ± 0.05	0.63 ± 0.05
1966 ± 3	0.67 ± 0.04	0.69 ± 0.04	0.62 ± 0.04	0.70 ± 0.04	0.66 ± 0.04	0.70 ± 0.04
2016 ± 3	0.74 ± 0.05	0.68 ± 0.05	0.76 ± 0.05	0.68 ± 0.05	0.69 ± 0.05	0.73 ± 0.05
2066 ± 3	0.72 ± 0.05	0.81 ± 0.05	0.75 ± 0.05	0.78 ± 0.05	0.70 ± 0.04	0.69 ± 0.04
2116 ± 3	0.76 ± 0.05	0.85 ± 0.06	0.77 ± 0.07	0.80 ± 0.05	0.75 ± 0.05	0.71 ± 0.05
2166 ± 3	0.81 ± 0.05	0.75 ± 0.05	0.77 ± 0.05	0.74 ± 0.05	0.71 ± 0.04	0.69 ± 0.04
2266 ± 3	0.82 ± 0.05	0.81 ± 0.05	0.75 ± 0.05	0.77 ± 0.05	0.72 ± 0.05	0.69 ± 0.04
2366 ± 3	0.88 ± 0.05	0.86 ± 0.05	0.77 ± 0.05	0.73 ± 0.05	0.75 ± 0.05	0.67 ± 0.04
2416 ± 3	0.82 ± 0.06	0.87 ± 0.06	0.78 ± 0.06	0.70 ± 0.05	0.64 ± 0.05	0.68 ± 0.05
2466 ± 3	0.89 ± 0.05	0.84 ± 0.05	0.81 ± 0.05	0.75 ± 0.05	0.63 ± 0.04	0.66 ± 0.04
2516 ± 3	0.94 ± 0.07	0.92 ± 0.07	0.80 ± 0.06	0.63 ± 0.06	0.65 ± 0.06	0.67 ± 0.06
2566 ± 3	0.95 ± 0.06	0.85 ± 0.06	0.81 ± 0.05	0.72 ± 0.05	0.66 ± 0.05	0.61 ± 0.04
2666 ± 3	0.95 ± 0.06	0.81 ± 0.05	0.80 ± 0.05	0.72 ± 0.05	0.59 ± 0.04	0.57 ± 0.04
2765 ± 3	0.86 ± 0.06	0.82 ± 0.05	0.69 ± 0.05	0.63 ± 0.04	0.52 ± 0.04	0.48 ± 0.04
2865 ± 3	0.86 ± 0.05	0.73 ± 0.05	0.68 ± 0.05	0.55 ± 0.04	0.46 ± 0.03	0.40 ± 0.03
2956 ± 3	0.78 ± 0.05	0.71 ± 0.05	0.63 ± 0.04	0.47 ± 0.03	0.43 ± 0.03	0.37 ± 0.03
3065 ± 3	0.75 ± 0.05	0.65 ± 0.04	0.54 ± 0.04	0.44 ± 0.03	0.365 ± 0.028	0.304 ± 0.025
3115 ± 3	0.75 ± 0.05	0.65 ± 0.04	0.53 ± 0.04	0.39 ± 0.04	0.353 ± 0.027	0.328 ± 0.027
3165 ± 3	0.68 ± 0.04	0.57 ± 0.04	0.51 ± 0.03	0.389 ± 0.029	0.335 ± 0.025	0.283 ± 0.023
3215 ± 3	0.63 ± 0.04	0.62 ± 0.04	0.46 ± 0.03	0.44 ± 0.03	0.325 ± 0.027	0.227 ± 0.023
3265 ± 3	0.60 ± 0.04	0.58 ± 0.04	0.50 ± 0.04	0.346 ± 0.029	0.314 ± 0.027	0.264 ± 0.025
3314 ± 3	0.70 ± 0.04	0.58 ± 0.04	0.44 ± 0.03	0.339 ± 0.026	0.308 ± 0.025	0.294 ± 0.024
3364 ± 3	0.69 ± 0.04	0.55 ± 0.04	0.42 ± 0.03	0.379 ± 0.029	0.302 ± 0.025	0.263 ± 0.023
3414 ± 3	0.64 ± 0.04	0.57 ± 0.04	0.48 ± 0.03	0.358 ± 0.028	0.328 ± 0.025	0.244 ± 0.022
3464 ± 3	0.62 ± 0.04	0.54 ± 0.04	0.423 ± 0.029	0.334 ± 0.025	0.288 ± 0.023	0.254 ± 0.021
3514 ± 3	0.63 ± 0.04	0.51 ± 0.03	0.47 ± 0.03	0.377 ± 0.026	0.303 ± 0.023	0.247 ± 0.021
3564 ± 3	0.61 ± 0.04	0.50 ± 0.04	0.48 ± 0.03	0.40 ± 0.03	0.338 ± 0.026	0.251 ± 0.023
3614 ± 3	0.62 ± 0.04	0.56 ± 0.04	0.48 ± 0.03	0.42 ± 0.03	0.330 ± 0.025	0.282 ± 0.024
3664 ± 3	0.62 ± 0.04	0.55 ± 0.04	0.50 ± 0.03	0.403 ± 0.029	0.344 ± 0.026	0.322 ± 0.025
3713 ± 3	0.58 ± 0.04	0.61 ± 0.04	0.55 ± 0.04	0.43 ± 0.03	0.340 ± 0.025	-
3763 ± 3	0.59 ± 0.04	0.57 ± 0.04	0.52 ± 0.03	0.46 ± 0.03	0.346 ± 0.025	-
3813 ± 3	0.57 ± 0.04	0.58 ± 0.04	0.54 ± 0.03	0.414 ± 0.029	-	-
3863 ± 3	0.67 ± 0.04	0.71 ± 0.04	0.59 ± 0.04	-	-	-
3913 ± 3	0.65 ± 0.04	0.64 ± 0.04	0.56 ± 0.03	-	-	-
3963 ± 3	0.69 ± 0.04	0.62 ± 0.04	0.57 ± 0.03	-	-	-
4013 ± 3	0.68 ± 0.04	0.61 ± 0.04	0.59 ± 0.04	-	-	-
4063 ± 3	0.68 ± 0.04	0.70 ± 0.04	-	-	-	-
4112 ± 3	0.70 ± 0.04	0.68 ± 0.04	-	-	-	-
4162 ± 3	0.77 ± 0.04	0.71 ± 0.04	-	-	-	-
4212 ± 3	0.73 ± 0.04	0.75 ± 0.04	-	-	-	-
4262 ± 3	0.73 ± 0.04	0.79 ± 0.05	-	-	-	-
4312 ± 3	0.73 ± 0.04	-	-	-	-	-
4362 ± 3	0.74 ± 0.04	-	-	-	-	-

E_{lab} (keV)	$d\sigma/d\Omega$ (mb/sr)					
	120°	130°	140°	150°	160°	170°
4411 ± 3	0.79 ± 0.04	-	-	-	-	-
4461 ± 3	0.82 ± 0.05	-	-	-	-	-
4511 ± 3	0.71 ± 0.04	-	-	-	-	-
4547 ± 3	0.74 ± 0.04	-	-	-	-	-
4597 ± 3	0.76 ± 0.04	-	-	-	-	-
4661 ± 3	0.75 ± 0.04	-	-	-	-	-

Table 9